64-10

BSD-TDR-63-256

The Effect of Geophysical and Geodetic Uncertainties at Launch Area on Ballistic Missile Impact Accuracy

22 JANUARY 1964

Prepared by
R. G. GORE

Prepared for COMMANDER
HEADQUARTERS, BALLISTIC SYSTEMS DIVISION
AIR FORCE SYSTEMS COMMAND
UNITED STATES AIR FORCE
Norton Air Force Base, California

SYSTEMS RESEARCH AND PLANNING DIVISION • AEROSPACE CORPORATION
CONTRACT NO. AF 04(695)-269

BSD-TDR-63-256

Report Number
TDR-269(4922)-2

THE EFFECT OF GEOPHYSICAL AND GEODETIC UNCERTAINTIES AT LAUNCH AREA ON BALLISTIC MISSILE IMPACT ACCURACY

R. G. Gore

22 January 1964

Contract No. AF04(695)-269

Systems Research and Planning Division
AEROSPACE CORPORATION
2400 East El Segundo Boulevard
El Segundo, California

Prepared for

COMMANDER
HEADQUARTERS, BALLISTIC SYSTEMS DIVISION
AIR FORCE SYSTEMS COMMAND
UNITED STATES AIR FORCE
Norton Air Force Base, California

BSD-TDR-63-256

Report Number
TDR-269(4922)-2

THE EFFECT OF GEOPHYSICAL AND GEODETIC UNCERTAINTIES AT LAUNCH AREA ON BALLISTIC MISSILE IMPACT ACCURACY

R. G. Gore

22 January 1964

This Technical Documentary Report has been reviewed and is approved for publication and dissemination but does not necessarily represent an official USAF position.

For Ballistic Systems Division
Air Force Systems Command:

MAURICE E. STUDEBAKER
Major, USAF
Deputy Chief, Guid Technology Div
Dir/Guidance and Control

For Systems Research and Planning
Division, Aerospace Corporation:

C. M. Price, Head
Astrodynamics Department

AEROSPACE CORPORATION
2400 East El Segundo Boulevard
El Segundo, California

ABSTRACT

The effects of uncertainties in the geophysical and geodetic parameters related to the establishment of ballistic missile launch sites on the impact accuracy of the ballistic missile are derived analytically. Curves of the derived impact miss coefficients are presented for radio- and inertially-guided missiles for ranges of 500 to 21,000 nautical miles and burnout angles of 5 to 90 degrees from the vertical.

CONTENTS

I. INTRODUCTION

This report documents a study of those geophysical and geodetic (G&G) phenomena which are pertinent to the establishment of a missile launch site. A study of this particular class of G&G effects is necessary for ascertaining their relationship to the ultimate accuracy of the ballistic weapon system. In particular, this relationship is relevant and valuable in the study of possible constraints on future weapon systems. This is not to under estimate the importance of these effects for present weapon systems; however, the determination of G&G launch area effects for presently well-defined systems can, and has been, adequately handled by direct computer simulation. The study of G&G effects for future weapon systems cannot be so easily simulated since much of the relevant information required by the computer is unspecified. The purpose of this report, then, will be to provide a study of the particular class of G&G effects associated with launch site development in sufficient generality to allow reasonably accurate estimates to be obtained for any missile system which might be considered. What is gained in generality will be, of course, lost in accuracy. For many studies of future systems, estimates of errors with an accuracy greater than ± 10 per cent is inappropriate and unwarranted; this guideline was maintained in conducting this study.

The G&G information which must be provided prior to the liftoff of a ballistic missile is the location of the launch site and the orientation in space of some nominal coordinate system. Consider, specifically, a right-handed orthogonal coordinate system whose origin is at the intended launch point; define one axis, the y axis, of this coordinate system as parallel to the radius vector from the center of the earth to the launch point; define the x axis as parallel to the plane defined by the intended velocity vector at burnout and the center of the earth; the z axis is thus defined by the requirement that the system be right-handed. This coordinate system just defined shall be termed the nominal coordinate system. Several unpleasant properties of

such a nominal coordinate system should be mentioned: (1) except at special points (the poles and equator) the y axis is not normal to any reference datum surfaces presently in use; and (2) most ballistic missile trajectories in practice are not coplanar due to the earth's rotation thus the burnout velocity vector does not lie in the xy plane.

Properties 1 and 2 above result from comparing an oblate, rotating earth (ORE) with a spherical, nonrotating earth (SNRE). A key assumption of this report will be that deviations caused by G&G effects from a trajectory traversed over an ORE can be approximated by similarly caused deviations from a trajectory traversed over a SNRE. A qualitative argument in support of this assumption may be made as follows: for ICBM's the differences between trajectories over an ORE and a SNRE are small as compared to the trajectories themselves; consequently, the deviations caused by small G&G effects for SNRE trajectories will differ from similarly generated deviations for ORE trajectories by a small perturbation in the already comparatively small difference between ORE and SNRE trajectories. The assumption that it is sufficient to treat SNRE trajectories removes the necessity of considering the disparities indicated by properties 1 and 2.

If the ICBM is considered to follow a specified trajectory in the nominal coordinate system, then the class of G&G uncertainties under consideration have, at liftoff, the effect of rigidly transforming the coordinate system in which the missile actually flies. There are six and only six independent transformations of the nominal coordinate system: three rotations about each of the axes; three translations along each of the axes. Each of these transformations can be identified as being generated by a particular G&G uncertainty as shown in Table 1.

Table 1.

Transformation	Corresponding G&G Uncertainty
Rotation about z axis	Deflection of the vertical uncertainty; component in trajectory plane
Translation along y axis	Elevation above reference ellipsoid uncertainty
Translation along x axis	Horizontal position uncertainty; down-range component
Rotation about x axis	Deflection of the vertical uncertainty; component perpendicular to trajectory plane
Rotation about y axis	Azimuth uncertainty
Translation along z axis	Horizontal position uncertainty; cross-range component

A complete evaluation of the effects of the above uncertainties requires that they be interpreted in terms of target miss of the missile. The required analysis may, for simplicity, be divided into two phases: Phase I, the analysis of the G&G effects through the powered portion of the missile flight to burnout at which the perturbation of the burnout conditions should be obtained; Phase II, the analysis of the effect of previously defined burnout perturbations on the free flight of the missile until impact. Re-entry conditions will be ignored under the assumption that deviations of the missile from the nominal re-entry point will produce an equal error in impact point. The analysis in Phase I will be considerably simplified by use of the facts that the geocentric angle between liftoff and burnout for most missiles is of the order of 5 degrees and the burnout height is generally of the order of 1/10, or less, of the earth's radius and consequently both quantities may frequently be ignored.

II. PHASE I ANALYSIS

From liftoff to burnout a missile is acted upon by the thrust force of the rocket engines, aerodynamic forces, and gravitational forces. The gravitational forces are wholly a function of position of the missile. The aerodynamic forces are strongly a function of time and only weakly a function of position. The thrust force can be a more complex function of time and position, since this force is controlled by the guidance system. Two basic categories of thrust guidance may be discriminated: (1) the thrust is controlled so as to conform to a predetermined acceleration program; such a process would be characteristic of an all-inertial guidance system and the thrust force is almost entirely a function of time; (2) the thrust is controlled in a manner which will maintain the missile on a predetermined trajectory; such a process requires a guidance system which can provide feedback control to the missiles, a process which is characteristic, ideally, of radio guidance systems and partly characteristic of astro-inertial and radio-inertial guidance systems. Since it will be shown that the analysis for missile systems of Category 2 may be obtained by a specialization of the results for Category 1 missile systems, the Category 1 missile systems will be considered first.

A. Category 1

If the position vector to the missile in the nominal coordinate system is denoted by $\vec{r}$, and time differentiation by dot's over the letter, then Category 1 systems involve the consideration of equations of the nature of (1).

$$\ddot{\vec{r}} = \vec{F}(t) + \vec{G}(\vec{r}) \qquad \dot{\vec{r}}(0) = 0, \quad \vec{r}(0) = 0 \qquad (1)$$

where $\vec{F}(t)$ represents the thrust and aerodynamic forces and $\vec{G}(\vec{r})$ represents the gravitational forces.

1. Deflection of the Vertical, Downrange Component $\delta_{||}$

Errors are created by this effect in the following manner: the angle α, between the thrust vector, whose magnitude is F(t), and the y axis is a function of time chosen so as to provide the proper burnout conditions; however, the angle α is actually measured throughout the flight with reference to a coordinate system rotated about the axis by $\delta_{||}$, see Figure 1.

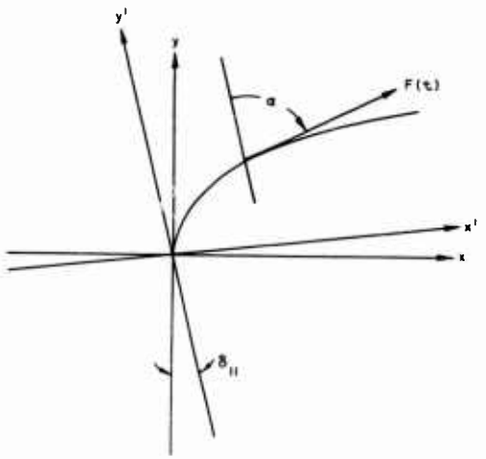

Figure 1.

The thrust components in the nominal system are thus:

$$F_x = \sin(\alpha - \delta_{||})\, F(t), \quad F_y = \cos(\alpha - \delta_{||})\, F(t) \qquad (2)$$

but $F_x^o = \sin\alpha\, F(t)$, $F_y^o = \cos\alpha\, F(t)$ where F_x^o, F_y^o are the components which were intended to be obtained, the nominal components. Equation (2) becomes then

$$F_x = \cos\delta_{||}\, F_x^o - \sin\delta_{||}\, F_y^o, \quad F_y = \cos\delta_{||}\, F_y^o + \sin\delta_{||}\, F_x^o \qquad (3)$$

Note that use has been made of a prior assumption that the xy plane contains the plane of the trajectory. For the sake of brevity, define the operators τ, τ^2 as:

$$\tau[f(t)] = \int_o^T f(t)dt, \quad \tau^2[f(t)] = \int_o^T dt \int_o^t f(\xi)\, d\xi \ .$$

The operator τ operating on any constant, c, gives $\tau[c] = c\,T$ and $\tau^2[c] = c\,(T^2/2)$, where T is the total time of integration; in this report T equals the time from liftoff to burnout of a missile. Then from Equation (1), utilizing $x(0) = y(0) = 0$, and representing a variable's value at burnout by a subscript B:

$$x_B = \tau^2[F_x(t) + G_x(x, y)], \quad y_B = \tau^2[F_y(t) + G_y(x, y)] \ . \qquad (4)$$

Combining (3) and (4) now gives:

$$\left.\begin{aligned} x_B &= \cos\delta_{\|}\,\tau^2[F_x^o(t)] - \sin\delta_{\|}\,\tau^2[F_y^o(t)] + \tau^2[G_x(x, y)] \\ y_B &= \cos\delta_{\|}\,\tau^2[F_y^o(t)] + \sin\delta_{\|}\,\tau^2[F_x^o(t)] + \tau^2[G_y(x, y)] \end{aligned}\right\} \qquad (5)$$

Noting that $\tau^2[F_x^o(t)] = x_B^o - \tau^2[G_x(x^o, y^o)]$,

$$\tau^2[F_y^o(t)] = y_B^o - \tau^2[G_y(x^o, y^o)] \qquad (6)$$

where x^o, y^o are the nominal coordinates, and anticipating small $\delta_{\|}$ so that $\cos\delta_{\|} = 1$, $\sin\delta_{\|} \doteq \delta_{\|}$, then (6) and (5) may be combined to give:

$$\begin{aligned} x_B &= x_B^o - \tau^2[G_x(x^o, y^o)] - \delta_{\|}\,y_B^o + \delta_{\|}\,\tau^2[G_y(x^o, y^o)] + \tau^2[G_x(x, y)] \\ y_B &= y_B^o - \tau^2[G_y(x^o, y^o)] + \delta_{\|}\,x_B^o - \delta_{\|}\,\tau^2[G_x(x^o, y^o)] + \tau^2[G_y(x, y)] \end{aligned} \qquad (7)$$

By changing the operator notation the velocity components are similarly derived:

$$\dot{x}_B = \dot{x}_B^o - \tau[G_x(x^o, y^o)] - \delta_{\|}\dot{y}_B^o + \delta_{\|}\tau[G_y(x^o, y^o)] + \tau[G_x(x, y)]$$
$$y_B = y_B^o - \tau[G_y(x^o, y^o)] + \delta_{\|}x_B^o - \delta_{\|}\tau[G_x(x^o, y^o)] + \tau[G_y(x, y)] \quad (8)$$

Now

$$G_x(x, y) - G_x(x^o, y^o) = \Delta x \left.\frac{\partial G_x}{\partial x}\right|_{\substack{x=x^o \\ y=y^o}} + \Delta y \left.\frac{\partial G_x}{\partial y}\right|_{\substack{x=x^o \\ y=y^o}} \equiv \Delta x\, G_{xx}^o + \Delta y\, G_{xy}^o$$

and similarly $G_y(x, y) - G_y(x^o, y^o) = \Delta x\, G_{yx}^o + \Delta y\, G_{yy}^o$ where $\Delta x = x - x^o$, $\Delta y = y - y^o$ as well as $\Delta\dot{x} = \dot{x} - \dot{x}^o$, $\Delta\dot{y} = \dot{y} - \dot{y}^o$. Equations (7) and (8) are now considerably simplified to

$$\left.\begin{aligned} \Delta x_B &= -\delta_{\|}\, y_B^o + \delta_{\|}\tau^2[G_y(x^o, y^o)] + \tau^2[\Delta x\, G_{xx}^o + \Delta y\, G_{xy}^o] \\ \Delta y_B &= \delta_{\|}\, x_B^o - \delta_{\|}\tau^2[G_x(x^o, y^o)] + \tau^2[\Delta x\, G_{yx}^o + \Delta y\, G_{yy}^o] \end{aligned}\right\} \quad (9)$$

$$\left.\begin{aligned} \Delta\dot{x}_B &= -\delta_{\|}\, \dot{y}_B^o + \delta_{\|}\tau[G_y(x^o, y^o)] + \tau[\Delta x\, G_{xx}^o + \Delta y\, G_{xy}^o] \\ \Delta\dot{y}_B &= \delta_{\|}\dot{x}_B^o - \delta_{\|}\tau[G_x(x^o, y^o)] + \tau[\Delta x\, G_{yx}^o + \Delta y\, G_{yy}^o] \end{aligned}\right\} \quad (10)$$

From Figure 2 the derivation for G_x, G_y, can be readily obtained:

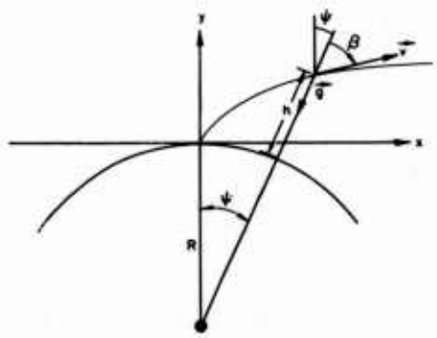

Figure 2.

$$G_x = - \frac{GM\, x^o}{\left[x^{o2} + (R + y^o)^2\right]^{3/2}} = - \frac{GM}{(R + h^o)^2} \sin \psi^o$$

$$G_y = - \frac{GM\,(y^o + R)}{\left[x^{o2} + (R + y^o)^2\right]^{3/2}} = - \frac{GM}{(R + h^o)^2} \cos \psi^o$$

and consequently

$$G^o_{xx} = \frac{-GM}{\left[x^{o2} + (R + y^o)^2\right]^{3/2}} + \frac{3\,GM\, x^{o2}}{\left[x^{o2} + (R + y^o)^2\right]^{5/2}}$$

$$= - \frac{GM}{(R + h^o)^3} \left[1 - 3 \sin^2 \psi^o\right]$$

$$G^o_{xy} = \frac{3\,GM\, x^o (R + y^o)}{\left[x^{o2} + (R + y^o)^2\right]^{5/2}} = \frac{GM}{(R + h^o)^3} (3 \sin \psi^o \cos \psi^o) = G^o_{yx}$$

$$G^o_{yy} = \frac{GM}{\left[x^{o2} + (R + y^o)^2\right]^{3/2}} + \frac{3GM\,(y^o + R)^2}{\left[x^{o2} + (R + y^o)^2\right]^{5/2}}$$

$$= - \frac{GM}{(R + h^o)^3} \left[1 - 3 \cos^2 \psi^o\right]$$

However, remembering h/R and ψ are small gives the more practical approximate relations, letting $\frac{GM}{R^2} = g_o$:

$$G_x \doteq 0,\ G_y \doteq -g_o,\ G^o_{xx} \doteq - \frac{g_o}{R},\ G^o_{xy} \doteq 0 = G^o_{yx},\ G_{yy} \doteq 2 \frac{g_o}{R} \qquad (11)$$

Equations (9) and (10) can thus be considerably simplified by the approximate relations in (11):

$$\left.\begin{aligned} \Delta x_B &\doteq -\delta_{\|}\, y^o_B - \delta_{\|}\, g_o \frac{T^2}{2} - g_o\, \tau^2 \left[\frac{\Delta x}{R}\right] \\ \Delta y_B &\doteq \delta_{\|}\, x^o_B + 2 g_o\, \tau^2 \left[\frac{\Delta y}{R}\right] \end{aligned}\right\} \qquad (12)$$

$$\left.\begin{aligned} \Delta\dot{x}_B &= -\delta_{\|}\dot{y}_B^o - \delta_{\|} g_o T - g_o t\tau \left[\frac{\Delta x}{R}\right] \\ \Delta\dot{y}_B &= \delta_{\|}\dot{x}_B^o + 2g_o\tau\left[\frac{\Delta y}{R}\right] \end{aligned}\right\} \qquad (13)$$

Now, from Figure 2,

$$y^o = (R + h^o)\cos\psi^o - R, \quad x^o = (R + h^o)\sin\psi^o. \qquad (14)$$

Equations (12) and (13) are essentially integral equations which converge quite rapidly for reasonable values of T; one iteration of (12) gives:

$$\Delta x_B = -\delta_{\|}\left[(R + h_B^o)\cos\psi_B^o - R\right] - \delta_{\|} g_o \frac{T^2}{2} - g_o\tau^2$$

$$\left\{-\delta_{\|}\left[\left(1 + \frac{h^o}{R}\right)\cos\psi^o - 1\right] - \delta_{\|}\frac{g_o}{R}\frac{T^2}{2} - g_o\tau^2\left[\frac{\Delta x}{R^2}\right]\right\} \qquad (15)$$

$$\Delta y_B = \delta_{\|}(R + h_B^o)\sin\psi_B^o + 2g_o\tau^2\left\{\delta_{\|}\left(1 + \frac{h^o}{R}\right)\sin\psi^o + 2\frac{g_o}{R}\tau^2\left[\frac{\Delta y}{R^2}\right]\right\}$$

The terms under the τ^2 operator in (15) are already of the order of terms previously neglected, hence:

$$\left.\begin{aligned} \Delta x_B &= -\delta_{\|}\left[h_B^o + g_o\frac{T^2}{2}\right] \\ \Delta y_B &= \delta_{\|} R\sin\psi_B^o \end{aligned}\right\} \qquad (16)$$

If (16) is substituted into (13) the terms under the τ operator are clearly negligible, giving:

$$\Delta\dot{x}_B = -\delta_{\|}\left[\dot{y}_B^o + g_o T\right] = -\delta_{\|}\left[v_B\cos(\beta_B^o + \psi_B^o) + g_o T\right]$$

$$\Delta\dot{y}_B = \delta_{\|}\dot{x}_B^o = \delta_{\|} v_B^o\sin(\beta_B^o + \psi_B^o) \qquad (17)$$

The relation between $\delta_{\|}$ and perturbations in the burnout conditions are given by (16) and (17) but in a clumsy reference system for the analysis in Phase II. More useful quantities would by $\Delta\psi$, Δh, $\Delta\beta$, Δv rather than Δx, Δy, $\Delta\dot{x}$, $\Delta\dot{y}$; the necessary relationships can be quickly derived using Figure 2:

$$\tan\psi = \frac{x}{R+y}, \quad d\psi = (R+h)^{-1}\left[\cos\psi\, dx - \sin\psi\, dy\right] \tag{18a}$$

$$(R+h)^2 = x^2 + (R+h)^2, \quad dh = \sin\psi\, dx + \cos\psi\, dy \tag{18b}$$

$$\tan(\beta+\psi) = \frac{\dot{x}}{\dot{y}}, \quad d\beta + d\psi = \frac{1}{v}\left[\cos(\beta+\psi)\, d\dot{x} - \sin(\beta+\psi)\, d\dot{y}\right] \tag{18c}$$

$$v^2 = \dot{x}^2 + \dot{y}^2, \quad dv = \sin(\beta+\psi)\, d\dot{x} + \cos(\beta+\psi)\, d\dot{y} \tag{18d}$$

Equations (16), (17) and (18) now give for burnout (T)

$$\Delta\psi = \delta_{\|}\left\{\frac{-h_B^o}{R+h_B^o}\cos\psi_B^o - \frac{g_o T^2}{2(R+h_B^o)}\cos\psi_B^o - \frac{R\sin^2\psi_B^o}{(R+h_B^o)}\right\} \doteq 0 \tag{19a}$$

$$\Delta h = \delta_{\|}\left\{-\sin\psi_B^o h_B^o - \sin\psi_B^o\frac{g_o T^2}{2} + R\sin\psi_B^o\cos\psi_B^o\right\} \doteq \delta_{\|} R\sin\psi_B^o \tag{19b}$$

$$\Delta\beta = \delta_{\|}\left\{-1 - \frac{g_o T}{v_B^o}\cos(\beta_B^o + \psi_B^o)\right\} \tag{19c}$$

$$\Delta v = -\delta_{\|}\, g_o T \sin(\beta_B^o + \psi_B^o) \tag{19d}$$

2. Elevation Uncertainty, ϵ

The effect of this uncertainty is essentially to translate the origin of the nominal coordinate system a distance ϵ along the y axis. The equations for x and y corresponding to (4), using the τ operators, are

$$x_B = \tau^2 [F_x(t) + G_x(x, y)], \quad y_B = \tau^2 [F_y(t) + G_y(x, y)] + \epsilon \qquad (20)$$

Noting that $F_x(t) = F_x^o(t)$, $F_y(t) = F_y^o(t)$ the integral equations for Δx, Δy may be derived in a fashion similar to that used in obtaining (9) and (10) to obtain

$$\Delta x_B = \tau^2 [\Delta x G_{xx}^o + \Delta y G_{xy}^o] \qquad (21)$$

$$\Delta y_B = \tau^2 [\Delta x G_{yx}^o + \Delta y G_{yy}^o] + \epsilon$$

$$\left.\begin{aligned} \Delta \dot{x}_B &= \tau [\Delta x G_{xx}^o + \Delta y G_{xy}^o] \\ \Delta \dot{y}_B &= \tau [\Delta x G_{yx}^o + \Delta y G_{yy}^o] \end{aligned}\right\} \qquad (22)$$

Equations (11) may be used to effect an immediate simplification in (21) and (22)

$$\left.\begin{aligned} \Delta x_B &= -g_o \tau^2 \left[\frac{\Delta x}{R}\right] \\ \Delta y_B &= \epsilon + 2 g_o \tau^2 \left[\frac{\Delta y}{R}\right] \end{aligned}\right\} \qquad (23)$$

$$\left.\begin{aligned} \Delta \dot{x}_B &= -g_o \tau \left[\frac{\Delta x}{R}\right] \\ \Delta \dot{y}_B &= 2 g_o \tau \left[\frac{\Delta y}{R}\right] \end{aligned}\right\} \qquad (24)$$

From (23) and (24) it is clear that

$$\Delta x \doteq 0 \qquad \Delta y \doteq \epsilon \qquad (25)$$

and hence

$$\Delta \dot{x} \doteq 0 \qquad \Delta \dot{y} \doteq 2 g_o \frac{\epsilon}{R} T \qquad (26)$$

Then, using Equations (18a, b, c, d) with (25) and (26) gives

$$\Delta\psi = \frac{1}{R + h_B} [- \sin \psi_B \, \epsilon] \doteq 0 \tag{27a}$$

$$\Delta h = \epsilon \cos \psi_B \doteq \epsilon \tag{27b}$$

$$\Delta\beta = - \frac{\epsilon}{R} \sin (\beta_B + \psi_B) \frac{2 g_o T}{v_B} \tag{27c}$$

$$\Delta v = \frac{\epsilon}{R} \cos (\beta_B + \psi_B) \, 2 g_o T \tag{27d}$$

3. Horizontal Position Uncertainty, Downrange Component, d

The effect of this uncertainty is essentially to translate the origin of the nominal coordinate system a distance d along the x axis. The equations for x and y now become

$$\left.\begin{aligned} x_B &= \tau^2 [F_x(t) + G_x(x, y)] + d \\ y_B &= \tau^2 [F_y(t) + G_y(x, y)] \\ \dot{x}_B &= \tau [F_x(t) + G_x(x, y)], \quad \dot{y}_B = \tau [F_y(t) + G_y(x, y)] \end{aligned}\right\} \tag{28}$$

Again noting that $F_x(t) = F_x^o(t)$, $F_y(t) = F_y^o(t)$ we obtain:

$$\left.\begin{aligned} \Delta x_B &= d + \tau^2 [\Delta x G_{xx}^o + \Delta y G_{xy}^o] \\ \Delta y_B &= \tau^2 [\Delta x G_{yx}^o + \Delta y G_{yy}^o] \end{aligned}\right\} \tag{29}$$

$$\left.\begin{aligned} \Delta \dot{x}_B &= \tau [\Delta x G_{xx}^o + \Delta y G_{xy}^o] \\ \Delta \dot{y}_B &= \tau [\Delta x G_{yx}^o + \Delta y G_{yy}^o] \end{aligned}\right\} \tag{30}$$

Using Equations (11), Equations (29) become

$$\left.\begin{aligned} \Delta x_B &= d - g_o \tau^2 \left[\frac{\Delta x}{R}\right] \doteq d \\ \Delta y_B &= 2 g_o \tau^2 \left[\frac{\Delta y}{R}\right] \doteq 0 \end{aligned}\right\} \tag{31}$$

Equations (31) in (30) give:

$$\left.\begin{aligned} \Delta \dot{x}_B &\doteq - g_o \tau \left[\frac{d}{R}\right] = - g_o \frac{d}{R} T \\ \Delta \dot{y}_B &\doteq 0 \end{aligned}\right\} \tag{32}$$

Equations (18a, b, c, d) may now be used to obtain:

$$\Delta \psi_B = \frac{d}{R + h_B} \cos \psi_B \doteq \frac{d}{R} \tag{33a}$$

$$\Delta h_B = d \sin \psi_B = 0 \tag{33b}$$

$$\Delta \beta_B = - \frac{d}{R} \left[1 + \frac{g_o T}{v_B} \cos (\beta_B + \psi_B)\right] \tag{33c}$$

$$\Delta v = - \frac{d}{R} g_o T \sin (\beta_B + \psi_B) \tag{33d}$$

4. Deflection of the Vertical Uncertainty, Crossrange Component, δ_1

Analysis of this effect is facilitated by introducing the artifice of letting the nominal trajectory plane make an angle θ with xy plane and later allowing θ to approach 0. From Figure 3,

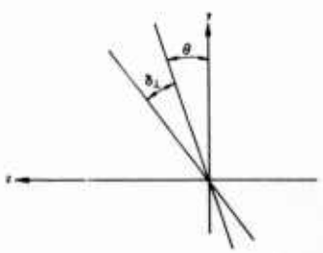

Figure 3.

$$\begin{aligned} F_z(t) &= F(t) \sin(\theta + \delta) \\ F_y(t) &= F(t) \cos(\theta + \delta) \\ F_x(t) &= F_x^o(t) \end{aligned} \tag{34}$$

Note that $F(t) \sin\theta = F_x^o(t)$ and $F(t)\cos\theta = F_y^o(t)$ thus Equation (34) gives

$$\left.\begin{aligned} F_z(t) &= F_z^o \cos\delta_\perp + F_y^o \sin\delta_\perp = F_z^o + \delta_\perp F_y^o \\ F_y(t) &= F_y^o \cos\delta_\perp - F_z^o \sin\delta_\perp = F_y^o - \delta_\perp F_x^o \\ F_x(t) &= F_x^o \end{aligned}\right\} \tag{35}$$

In the operator notation, we have:

$$x_B = \tau^2[F_x(t) + G_x(x, y, z)], \quad y_B = \tau^2[F_y(t) + G_y(x, y, z)]$$

$$z_B = \tau^2[F_z(t) + G_z(x, y, z)] \tag{36}$$

plus

$$\begin{aligned} \tau^2[F_x^o] &= x_B^o - \tau^2[G_x(x^o, y^o, z^o)] \\ \tau^2[F_y^o] &= y_B^o - \tau^2[G_y(x^o, y^o, z^o)] \\ \tau^2[F_z^o] &= z_B^o - \tau^2[G_z(x^o, y^o, z^o)] \end{aligned} \tag{37}$$

Remembering that $G_x(x, y, z) - G_x(x^o, y^o, z^o) = \Delta x\, G_{xx}^o + \Delta y\, G_{xy}^o + \Delta z\, G_{xz}^o$, etc., and using (37) and (35) in (36) Equations (38) are obtained:

$$\begin{aligned} \Delta x_B &= \tau^2[\Delta x\, G_{xx}^o + \Delta y\, G_{xy}^o + \Delta z\, G_{xz}^o] \\ \Delta y_B &= -\delta_\perp z_B^o + \delta_\perp \tau^2[G_z(x^o, y^o, z^o)] + \tau^2[\Delta x\, G_{yx}^o + \Delta y\, G_{yy}^o + \Delta z\, G_{zy}^o] \\ \Delta z_B &= \delta_\perp y_B^o - \delta_\perp \tau^2[G_y(x^o, y^o, z^o)] + \tau^2[\Delta x\, G_{zx}^o + \Delta y\, G_{zy}^o + \Delta z\, G_{zz}^o] \end{aligned} \tag{38}$$

A similar development replacing τ^2 with τ gives

$$\Delta\dot{x} = \tau\left[\Delta x\, G^o_{xx} + \Delta y\, G^o_{xy} + \Delta z\, G^o_{xz}\right]$$

$$\Delta\dot{y} = -\delta_\perp \dot{z}^o_B + \delta_\perp \tau\left[G_z(x^o, y^o, z^o)\right] + \tau\left[\Delta x\, G^o_{yx} + \Delta y\, G^o_{yy} + \Delta z\, G^o_{yz}\right]$$

$$\Delta\dot{z} = \delta_\perp \dot{y}^o_B - \delta_\perp \tau\left[G_y(x^o, y^o, z^o)\right] + \tau\left[\Delta x\, G^o_{zx} + \Delta y\, G^o_{zy} + \Delta z\, G^o_{zz}\right] \tag{39}$$

Allow θ to approach zero; now z^o, $\dot{z}^o$, $G_z(x^o, y^o, z^o) = 0$ and since

$$G^o_{xz} = \frac{3\,GM\,x^o z^o}{\left[x^{o2} + (R + y^o)^2 + z^{o2}\right]^{5/2}} = G^o_{zx},$$

$$G^o_{yz} = \frac{3\,GM(R + y^o)\,z^o}{\left[x^2 + (R + y^o)^2 + z^{o2}\right]^{5/2}} = G^o_{zy}$$

$$G^o_{zz} = -\frac{GM}{\left[x^{o2} + (R+y)^2 + z^{o2}\right]^{3/2}} + \frac{3\,GM\,z^2}{\left[x^2 + (R + y)^2 + z^2\right]^{5/2}}$$

we also have, in addition to (11),

$$G^o_{xz} = G^o_{yz} = G^o_{zy} = G^o_{zx} = 0, \quad G^o_{zz} \doteq -\frac{g_o}{R} \tag{40}$$

Using these results and Equations (11), Equations (38) and (39) simplify to:

$$\Delta x_B = -g_o \tau^2 \left[\frac{\Delta x}{R}\right] \doteq 0$$

$$\Delta y_B = 2 g_o \tau^2 \left[\frac{\Delta y}{R}\right] \doteq 0$$

$$\Delta x_B = \delta_\perp y^o_B + g_o \delta_\perp \frac{T^2}{2} - g_o \tau^2 \left[\frac{\Delta z}{R}\right] \tag{41}$$

$$= \delta_\perp \left[y^o_B + g_o \frac{T^2}{2}\right]$$

and using (41) in (39)

$$\begin{aligned} \Delta\dot{x} &= 0 \\ \Delta\dot{y} &= 0 \\ \Delta\dot{z} &= \delta_\perp \dot{y}_B^o + \delta_\perp g_o T - g_o \tau \left[\frac{\Delta z}{R}\right] \end{aligned} \tag{42}$$

Moreover $y^o = (R + h)\cos\psi - R \doteq h$ so that

$$\frac{\Delta z}{R} \doteq \frac{h_B}{R} + \frac{g_o}{R}\frac{T^2}{2} \doteq 0$$

and hence

$$\begin{aligned} \Delta\dot{z} &= \delta_\perp \left[\dot{y}_B^o + g_o T\right] \\ \Delta z &= \delta_\perp \left[h_P + \frac{g_o}{2} T^2\right] \end{aligned} \tag{43}$$

For small x, Δz is the crossrange displacement at burnout; however, $\Delta\dot{z}$ can most readily be handled when translated into azimuth uncertainty. Assume first that the trajectory plane makes an angle A_z with the xy plane, and that the velocity vector lies wholly in the trajectory plane, then

$$\tan A_z = \frac{\dot{z}_o}{\dot{x}_o}$$

using

$$\dot{x}_o = v \sin(\beta + \psi) \cos A_z$$

and

$$\dot{z}_o = v \sin(\beta + \psi) \sin A_z$$

$$dA_z = \frac{1}{v \sin(\beta + \psi)} \left(\cos A_z \, d\dot{z}_o - \sin A_z \, d\dot{x}_o\right)$$

and now letting $A_z = 0$

$$\Delta A_z = \frac{\Delta \dot{z}}{v \sin (\beta + \psi)} \tag{44}$$

The other burnout parameters remain essentially unaltered by $\Delta \dot{z}$ when $A_z = 0$. The ΔA_z in (44) is the variation in azimuth at the liftoff point; for the later analysis the azimuth perturbation at burnout is desired. Consider Figure 4: $\vec{v}$ is the nominal velocity vector which lies wholly in the xy plane; $\vec{v}'$ is the velocity vector with ψ, β, and magnitude equal to $\vec{v}$, which is however rotated from $\vec{v}$ through the angle ΔA_z about the y axis. From spherical trigonometry

$$\frac{\sin \Delta A_z}{\sin b} = \frac{\sin \Delta A_{z_B}}{\sin (\beta + \psi)}$$

and

$$\cos b = \cos (\beta + \psi) \cos \psi + \sin (\beta + \psi) \sin \psi \cos \Delta A_z$$

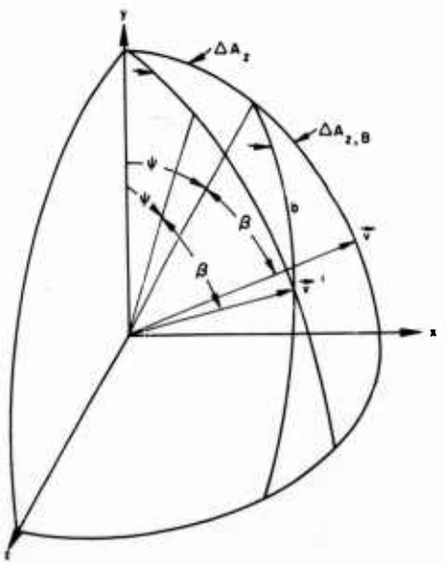

Figure 4.

For small ΔA_z, cos b = cos β and therefore

$$\sin \Delta A_{z,B} = \frac{\sin (\beta + \psi)}{\sin \beta} \sin \Delta A_z$$

or

$$\Delta A_{z,B} = \frac{\sin (\beta + \psi)}{\sin \beta} \Delta A_z \tag{45}$$

$\Delta A_{z,B}$ is the desired perturbation of the azimuth at burnout. Putting (44) in (45) gives, including the subscript B now for conformity with the previous results:

$$\Delta A_{z,B} = \frac{\Delta z_B}{v_B \sin \beta_B} \tag{46}$$

Now $y_B^o = v_B \cos (\beta_B + \psi_B)$, so we have

$$\Delta A_z = \delta_\perp \left[\frac{\cos (\beta_B + \psi)}{\sin \beta_B} + \frac{g_o T}{v_B \sin \beta_B} \right] \tag{47}$$

5. Azimuth Uncertainty, α

This uncertainty manifests itself by rotating the trajectory plane from the nominal xy plane by an angle α about the y axis. The thrust functions may be immediately written as

$$F_x(t) = F_x^o(t) - \alpha F_z^o(t)$$

$$F_y(t) = F_y^o(t)$$

$$F_z(t) = F_z^o(t) + \alpha F_x^o(t)$$

and by a development similar to previous derivations in this report

$$\begin{aligned}
\Delta x_B &= \alpha \tau^2 [G_z^o(x, y, z)] + \tau^2 [\Delta x G_{xx}^o + \Delta y G_{xy}^o + \Delta z G_{xz}^o] - \alpha z_B^o \\
\Delta y_B &= \tau^2 [\Delta x G_{yx}^o + \Delta y G_{yy}^o + \Delta z G_{yz}^o] \\
\Delta z_B &= \alpha x_B^o - \alpha \tau^2 [G_x^o(x, y, z)] + \tau^2 [\Delta x G_{zx}^o + \Delta y G_{zy}^o + \Delta z G_{zz}^o]
\end{aligned} \tag{48}$$

$$\Delta\dot{x}_B = -\alpha\dot{z}_B^o + \alpha\tau\left[G_z^o(x, y, z)\right] + \tau^2\left[\Delta x\, G_{xx}^o + \Delta y\, G_{xy}^o + \Delta z\, G_{xz}^o\right]$$

$$\Delta\dot{y}_B = \tau\left[\Delta\dot{x}\, G_{yx}^o + \Delta y\, G_{yy}^o + \Delta z\, G_{yz}^o\right] \qquad (49)$$

$$\Delta z_B = \alpha x_B^o - \alpha\tau\left[G_x^o(x, y, z)\right] + \tau\left[\Delta x\, G_{zx}^o + \Delta y\, G_{zy}^o + \Delta z\, G_{zz}^o\right]$$

Now using Equations (11) and (40) to simplify (48) and (49)

$$\left.\begin{aligned} \Delta x_B &= -g_o\tau^2\left[\frac{\Delta x}{R}\right] \doteq 0 \\ \Delta y_B &= 2g_o\tau^2\left[\frac{\Delta y}{R}\right] \doteq 0 \\ \Delta z_B &= \alpha x_B^o - g_o\tau^2\left[\frac{\Delta z}{R}\right] \doteq \alpha(R + h_B)\sin\psi_B \doteq \alpha R\sin\psi_B \end{aligned}\right\} \qquad (50)$$

$$\left.\begin{aligned} \Delta\dot{x}_B &= -g_o\tau\left[\frac{\Delta x}{R}\right] \doteq 0 \\ \Delta\dot{y}_B &= 2g_o\tau\left[\frac{\Delta y}{R}\right] \doteq 0 \\ \Delta\dot{z}_B &= \alpha\dot{x}_B^o - g_o\tau\left[\frac{\Delta z}{R}\right] \doteq \alpha v_B\sin(\beta_B + \psi_B) \end{aligned}\right\} \qquad (51)$$

From (46) and (51)

$$\Delta A_{z,B} = \alpha\,\frac{\sin(\beta + \psi)}{\sin\beta} \qquad (52)$$

6. Horizontal Position Uncertainty, Crossrange Component, c

This uncertainty has the effect of translating the actual coordinate system a distance c from the nominal coordinate system along the z axis. The basic equations for the coordinates are thus

$$x_B = \tau^2\left[F_x^o(t) + G_x(x, y, z)\right]$$

$$y_B = \tau^2\left[F_y^o(t) + G_y(x, y, z)\right]$$

$$z_B = \tau^2\left[F_z^o(t) + G_z(x, y, z)\right] + c$$

B. Category 2

Category 2 missile systems, those with feedback to maintain themselves upon a given trajectory, behave only as if the nominal coordinate system were rigidly transformed by the G&G effect; other dynamic considerations which arise from the fact that the missile experiences a different from nominal gravity field are removed by the feedback in the guidance systems, i.e., the missile is constrained to move exactly along the nominal trajectory in the transformed coordinate system. The results of the analysis for Category 1 missile systems can thus be used for Category 2 systems by removing the gravity effects; letting $g_o = 0$.

The results of the Phase I analysis are summarized in Table 2.

Table 2.

Geodetic and Geophysical Uncertainty	Burnout Perturbation/ G&G Uncertainty	Category 1	Category 2
Deflection of the Vertical Downrange Comp., $\delta_{\|\|}$	$\frac{\Delta\psi}{\delta_{\|\|}} =$	0	0
	$\frac{\Delta h}{\delta_{\|\|}} =$	$R \sin \psi$	$R \sin \psi$
	$\frac{\Delta\beta}{\delta_{\|\|}} =$	$-\left[1 + \frac{g_o T}{v} \cos(\beta+\psi)\right]$	-1
	$\frac{\Delta v}{\delta_{\|\|}} =$	$-g_o T \sin(\beta+\psi)$	0
	$\frac{\Delta A^o}{\delta_{\|\|}} =$	0	0
	$\frac{\Delta z}{\delta_{\|\|}} =$	0	0
Elevation Uncertainty, ϵ	$\frac{\Delta\psi}{\epsilon} =$	0	0
	$\frac{\Delta h}{\epsilon} =$	1	1
	$\frac{\Delta\beta}{\epsilon} =$	$-\frac{2 g_o T}{v R} \sin(\beta+\psi)$	0
	$\frac{\Delta v}{\epsilon} =$	$\frac{2 g_o T}{R} \cos(\beta+\psi)$	0
	$\frac{\Delta A^o}{\epsilon} =$	0	0
	$\frac{\Delta z}{\epsilon} =$	0	0

Table 2. (Continued)

Geodetic and Geophysical Uncertainty	Burnout Perturbation/ G&G Uncertainty	Category 1	Category 2
Horizontal Position Downrange Comp., d	$\frac{\Delta\psi}{d} =$	$\frac{1}{R}$	$\frac{1}{R}$
	$\frac{\Delta h}{d} =$	0	0
	$\frac{\Delta\beta}{d} =$	$-\frac{1}{R}\left[1+\frac{g_o T}{v}\cos(\beta+\psi)\right.$	$-\frac{1}{R}$
	$\frac{\Delta v}{d} =$	$-\frac{g_o T}{R}\sin(\beta+\psi)$	0
	$\frac{\Delta A^o}{d} =$	0	0
	$\frac{\Delta z}{d} =$	0	0
Deflection of the Vertical Crossrange Component, $\delta_\perp$	$\frac{\Delta\psi}{\delta_\perp} =$	0	0
	$\frac{\Delta h}{\delta_\perp} =$	0	0
	$\frac{\Delta\beta}{\delta_\perp} =$	0	0
	$\frac{\Delta v}{\delta_\perp} =$	0	0
	$\frac{\Delta A^o}{\delta_\perp} =$	$\frac{\cos(\beta+\psi)}{\sin\beta}+\frac{g_o T}{v\sin\beta}$	$\frac{\cos(\beta+\psi)}{\sin\beta}$
	$\frac{\Delta z}{\delta_\perp} =$	$h+\frac{g_o}{2}T^2$	h

Table 2. (Continued)

Geodetic and Geophysical Uncertainty	Burnout Perturbation/ G&G Uncertainty	Category 1	Category 2
Azimuth Uncertainty, α	$\frac{\Delta\psi}{\alpha}$ =	0	0
	$\frac{\Delta h}{\alpha}$ =	0	0
	$\frac{\Delta\beta}{\alpha}$ =	0	0
	$\frac{\Delta v}{\alpha}$ =	0	0
	$\frac{\Delta A^o}{\alpha}$ =	$\frac{\sin(\beta+\psi)}{\sin\beta}$	$\frac{\sin(\beta+\psi)}{\sin\beta}$
	$\frac{\Delta z}{\alpha}$ =	$R \sin\psi$	$R \sin\psi$
Horizontal Position Crossrange Component, c	$\frac{\Delta\psi}{c}$ =	0	0
	$\frac{\Delta h}{c}$ =	0	0
	$\frac{\Delta\beta}{c}$ =	0	0
	$\frac{\Delta v}{c}$ =	0	0
	$\frac{\Delta A^o}{c}$ =	$\frac{-g_o T}{R v \sin\beta}$	0
	$\frac{\Delta z}{c}$ =	1	1

III. PHASE II ANALYSIS

A complete analysis of G&G launch area effects requires that these effects be interpretable in terms of target miss. The Phase I analysis transformed the launch area uncertainties to uncertainties in burnout conditions. The analysis of this section will concern itself with transforming burnout uncertainties to target impact uncertainties. For the Phase II analysis as in the Phase I analysis the assumption is maintained that a spherical nonrotating earth is a sufficiently close approximation to reality to provide the desired results within the approximate 10 per cent guideline mentioned earlier.

The Phase I analysis found that launch area G&G uncertainties were interpretable in terms of six quantities: $\Delta\psi$, the variation in the geocentric downrange burnout angle; Δh, the variation in the burnout height above the sphere; $\Delta\beta$, the variation in the angle the burnout velocity vector makes with the radius vector at burnout; Δv, the variation in the burnout velocity; ΔA_z^o, the variation in the angle the plane of the trajectory makes with the meridional plane at burnout; Δz, the variation in the position of the burnout point measured perpendicularly to the plane of the trajectory. The first four quantities $\Delta\psi$, Δh, $\Delta\beta$, Δv all are perturbations in the plane of the nominal trajectory and consequently for a nonrotating earth these perturbations should only produce impact errors in the nominal trajectory plane. The component of impact error in the nominal trajectory plane is generally, and will be here, termed downrange miss. The latter two burnout variations, ΔA_z^o, Δz, are burnout perturbations out of the trajectory plane and consequently can be expected to produce impact errors out of the nominal trajectory plane. The component of impact error measured from the nominal trajectory plane is generally termed the crossrange error. The Phase II analysis thus naturally subdivides into the two categories: downrange miss and crossrange miss.

A. Downrange Miss

The simplest approach to analyzing the inplane burnout variations turns out to be the use of the ballistic missile "hit equation"

$$\frac{r_o}{r_f} = \frac{1 - \cos \phi}{\frac{r_o v^2}{GM} \sin^2 \beta} + \frac{\sin (\beta - \phi)}{\sin \beta} \qquad (58)$$

where the quantities are as defined in Figure 5.

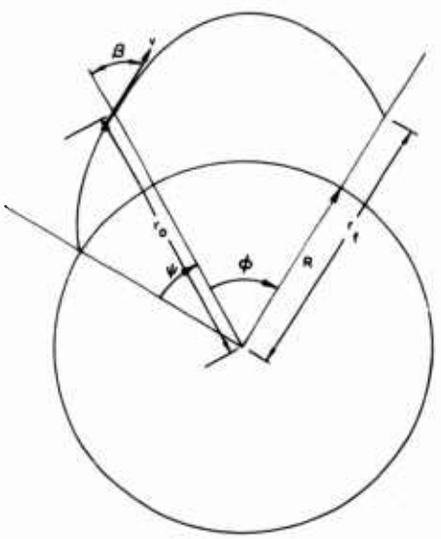

Figure 5.

For most ballistic missiles, if h is the burnout height, $r_o = R + h$, and $r_f = R$. Let $GM \equiv \mu$ for the sake of convenience then (58) becomes

$$(R + h) \frac{v^2}{\mu} \sin \beta \left[\left(1 + \frac{h}{R} \right) \sin \beta - \sin (\beta - \phi) \right] = 1 - \cos \phi \qquad (59)$$

Since the downrange miss is just $R\Delta\phi$, miss coefficients for h, β, v may immediately be obtained by implicitly differentiating (59) with respect to h, β, v, and ϕ and then substituting

$$(R+h)\,\frac{v^2}{\mu} = \frac{1-\cos\phi}{\sin\beta\left[\left(1+\frac{h}{R}\right)\sin\beta - \sin(\beta-\phi)\right]} \tag{60}$$

into the resulting expressions to remove the velocity dependence. This process gives:

$$MD_h = R\,\frac{\partial\phi}{\partial h} = \frac{2\sin\beta - \frac{R}{R+h}\sin(\beta-\phi)}{\cos\beta + \frac{h}{R}\sin\beta\,\frac{\sin\phi}{1-\cos\phi}} \tag{61}$$

$$MD_\beta = R\,\frac{\partial\phi}{\partial\beta} = R\,\frac{2\cos\beta\left(1+\frac{h}{R}\right) - \frac{\sin(2\beta-\phi)}{\sin\beta}}{\cos\beta + \frac{h}{R}\sin\beta\,\frac{\sin\phi}{1-\cos\phi}} \tag{62}$$

$$MD_v = R\frac{\partial\phi}{\partial v} = \frac{R}{v}\,\frac{2\left[\left(1+\frac{h}{R}\right)\sin\beta - \sin(\beta-\phi)\right]}{\cos\beta + \frac{h}{R}\sin\beta\,\frac{\sin\phi}{1-\cos\phi}} \tag{63}$$

From Figure 5 it is clear that

$$MD_\psi = R\,\frac{\partial\phi}{\partial\psi} = R \tag{64}$$

B. Crossrange Miss

For a spherical nonrotating earth the trace of the missile's trajectory on the surface of the earth is a great circle and thus the problem of determining crossrange miss becomes one of spherical trigonometry. With no loss in generality a spherical coordinate system may be adopted whose equatorial plane includes the nominal trajectory plane. Figure 6 should serve to clarify the particular coordinate system used. In Figure 6 the point B is the nominal burnout point projection; B' is the actual burnout

point projected onto the sphere; ϕ is the geocentric range angle as in Figure 5; A' is the actual burnout azimuth at B'. The point I is the nominal impact point and I' is the actual impact point. From the previous definitions $\Delta\theta$ is the crossrange miss, and $\Delta\lambda$ is the downrange miss.

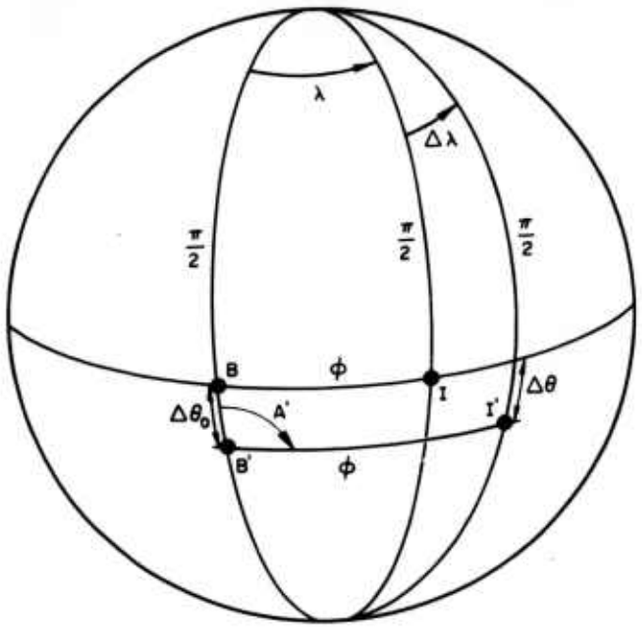

Figure 6.

The cosine law of spherical trigonometry gives:

$$\cos\left(\Delta\theta + \frac{\pi}{2}\right) = \cos\left(\frac{\pi}{2} + \Delta\theta_o\right)\cos\phi + \sin\left(\frac{\pi}{2} + \Delta\theta_o\right)\sin\phi\cos A' \tag{65}$$

Now

$$\Delta\theta_o = \frac{\Delta z}{R+h}$$

and

$$A' = \frac{\pi}{2} + \Delta A_z^o$$

where Δz, ΔA are both small.

Equation (65) becomes

$$\sin \Delta\theta = \sin \frac{\Delta z}{R+h} \cos \phi + \cos \frac{\Delta z}{R+h} \sin \phi \sin \Delta A_z^o \qquad (66)$$

and for small quantities

$$\Delta\theta \doteq \frac{\Delta z}{R+h} \cos \phi + \Delta A_z^o \sin \phi \qquad (67)$$

The crossrange miss, MC, is $R\Delta\theta$ so

$$MC_{\Delta z} = \Delta z \frac{R}{R+h} \cos \phi$$

$$MC_{\Delta A_z^o} = + R \Delta A_z^o \sin \phi \qquad (68)$$

The downrange miss can be obtained by solving for $\Delta\lambda$. The sine law gives

$$\frac{\sin (\lambda + \Delta\lambda)}{\sin \phi} = \frac{\sin\left(\frac{\pi}{2} + \Delta A\right)}{\sin\left(\frac{\pi}{2} + \Delta\theta\right)}$$

and, consequently, keeping only first order terms in $\Delta\lambda$ and noting that $\lambda \equiv \phi$ gives

$$\cos \Delta\theta \left[\sin \phi + \Delta\lambda \cos \phi\right] = \sin \phi \cos \Delta A \qquad (70)$$

From (70) if only first order terms in ΔA and $\Delta\theta$ are kept, $\Delta\lambda = 0$. Therefore, $\Delta\lambda$, the downrange miss attributable to Δz and ΔA_z^o, is of second order in these uncertainties and may thus be ignored. Table 3 summarizes the results of the Phase II analysis.

C. Numerical Analysis of G&G Uncertainties

The results tabulated in Tables 2 and 3 could be combined to give analytical representations for target miss per G&G uncertainty. The results of such a recombination would be sufficiently complicated as to preclude any useful understanding of the relationship between G&G effects

Table 3.

Burnout Parameter	Downrange Miss Coefficient	Crossrange Miss Coefficient
h	$MD_h = \dfrac{2 \sin \beta - \dfrac{R}{R+h} \sin (\beta + \phi)}{\cos \beta + \dfrac{h}{R} \sin \beta \dfrac{\sin \phi}{1 - \cos \phi}}$	$MC_h = 0$
β	$MD_\beta = \dfrac{2 \cos \beta \left(1 + \dfrac{h}{R}\right) - \dfrac{\sin (2\beta - \phi)}{\sin \beta}}{\cos \beta + \dfrac{h}{R} \sin \beta \dfrac{\sin \phi}{1 - \cos \phi}}$	$MC_\beta = 0$
v	$MD_v = \dfrac{R}{v} \dfrac{2 \left(1 + \dfrac{h}{R}\right) \sin \beta - \sin (\beta - \phi)}{\cos \beta + \dfrac{h}{R} \sin \beta \dfrac{\sin \phi}{1 - \cos \phi}}$	$MC_v = 0$
ψ	$MD_\psi = R$	$MC_\psi = 0$
Δz	$MD_{\Delta z} = 0$	$MC_{\Delta z} = \cos \phi$
ΔA_z^o	$MD_{\Delta A_z^o} = 0$	$MC_{\Delta A_z^o} = R \sin \phi$

at the launch area and target miss. Consequently, the results of the previous sections were used to generate curves giving the value of target miss/G&G uncertainty over wide limits of burnout angle and missile range.

The expressions in Tables 2 and 3 are functions not only of the burnout angle, β, and range, ϕ but also of h, ψ, v, and T: burnout height, downrange burnout geocentric angle, burnout velocity, and total time of powered flight. Inclusion of these latter variables as independent variables in the numerical analysis would increase the extent of the required analysis to a point where any generality would be lost. Accordingly, an attempt was made to specify these variables either as constants or as functions of β and ϕ.* For the other variables h, ψ, and T, a series of sample ICBM trajectories were examined. The time, T, was found to weakly vary over large variations in range and burnout angle and consequently a constant value, T = 185 sec, was utilized for this analysis. Sinch h and ψ were found to vary over ranges of 500,000 - 1,500,000 ft and 4 - 5 deg, respectively, power series expansions were made considering h, ψ to be functions of θ and ϕ. The series expansions were then made to conform exactly to six different sample ICBM trajectories, three each at 5500 nautical miles and 7500 nautical miles; each trajectory had a different burnout angle. These trajectories were felt to be representative of most operational ICBM trajectories of interest. The resulting expansions in h and ψ were used for those cases in which the expansions gave values within the, essentially, arbitrary bounds of 500,000 ft $\leq$ h $\leq$ 1,500,000 ft, $1^{o} \leq \psi \leq 10^{o}$; if the value of h or ψ exceeded these bounds, the value used in the computation was the relevant upper or lower bound. These more or less artificial constraints were found to be necessary for those values of β and ϕ widely removed from the region in which the expansions were defined.

For $\phi > \pi$ (R > 10,800 naut mi) the lower bound for h ..... 500,000 feet. .....was used entirely, since ballistic systems utilized for these ranges would be under severe propulsion requirements and, therefore, the

*From the "hit equation," (1), burnout velocity can immediately be determined as a function of θ and ϕ.

powered flight trajectory might be expected to be shaped, as nearly as possible, horizontally. For these ranges ψ was set equal to 10 degrees again because the severe energy requirements would engender a powered trajectory extended to the limit downrange.

The curves so generated are given below in the following order:

1. Inertially guided systems, 500 - 10,000 naut mi
2. Inertially guided systems, 10,000 - 22,000 naut mi
3. Radio guided systems, 500 - 10,000 naut mi
4. Radio guided systems, 10,000 - 22,000 naut mi

Curves of equal burnout velocity have also been included in the plots listed above as an aid in analysis. For ranges in excess of 10,000 nautical miles certain portions of the β, R plot are inadmissiable for ballistic missiles; these regions are also indicated on the appropriate contour plots.

Index of Launch Area Uncertainty Contour Plots

Solid Contours give Target Miss/Uncertainty as Specified in Table Below

Dashed Contours give the Burnout Velocity Requirement in Feet/Second

Guidance Type	Launch Area Uncertainty	Contours given in Units of:	Contour Plot No.
	500 - 10,500 Nautical Miles		
Inertial	Deflection of the Vertical ($\delta_{\parallel}$)	M_{DR} (ft)/$\delta_{\parallel}$ ($\widehat{sec}$)	1
Inertial	Elevation above Ellipsoid (ϵ)	M_{DR} (ft)/ϵ (ft)	2
Inertial	Horizontal Position (d)	M_{DR} (ft)/d (ft)	3
Inertial	Deflection of the Vertical ($\delta_{\perp}$)	M_{CR} (ft)/$\delta_{\perp}$ ($\widehat{sec}$)	4
Inertial	Horizontal Position (c)	M_{CR} (ft)/c (ft)	5
Inertial	Azimuth (A_z)	M_{CR} (ft)/A_z ($\widehat{sec}$)	6
	10,000 - 22,000 Nautical Miles		
Inertial	Deflection of the Vertical ($\delta_{\parallel}$)	M_{DR} (ft)/$\delta_{\parallel}$ ($\widehat{sec}$)	7
Inertial	Elevation above Ellipsoid (ϵ)	M_{DR} (ft)/ϵ (ft)	8
Inertial	Horizontal Position (d)	M_{DR} (ft)/d (ft)	9
Inertial	Deflection of the Vertical ($\delta_{\perp}$)	M_{CR} (ft)/$\delta_{\perp}$ ($\widehat{sec}$)	10
Inertial	Horizontal Position (c)	M_{CR} (ft)/c (ft)	11
Inertial	Azimuth (A_z)	M_{CR} (ft)/A_z ($\widehat{sec}$)	12

Guidance Type	Launch Area Uncertainty	Contours given in Units of:	Contour Plot No.
	500 - 10,500 Nautical Miles		
Radio	Deflection of the Vertical ($\delta_{\parallel}$)	M_{DR} (ft)/$\delta_{\parallel}$ ($\widehat{sec}$)	13
Radio	Elevation above Ellipsoid (ϵ)	M_{DR} (ft)/ϵ (ft)	14
Radio	Horizontal Position (d)	M_{DR} (ft)/d (ft)	15
Radio	Deflection of the Vertical ($\delta_{\perp}$)	M_{CR} (ft)/$\delta_{\perp}$ ($\widehat{sec}$)	16
Radio	Horizontal Position (c)	M_{CR} (ft)/c (ft)	17
Radio	Azimuth (A_z)	M_{CR} (ft)/A_z ($\widehat{sec}$)	18
	10,000 - 22,000 Nautical Miles		
Radio	Deflection of the Vertical ($\delta_{\parallel}$)	M_{DR} (ft)/$\delta_{\parallel}$ ($\widehat{sec}$)	19
Radio	Elevation above Ellipsoid (ϵ)	M_{DR} (ft)/ϵ (ft)	20
Radio	Horizontal Position (d)	M_{DR} (ft)/d (ft)	21
Radio	Deflection of the Vertical ($\delta_{\perp}$)	M_{CR} (ft)/$\delta_{\perp}$ ($\widehat{sec}$)	22
Radio	Horizontal Position (c)	M_{CR} (ft)/c (ft)	23
Radio	Azimuth (A_z)	M_{CR} (ft)/A_z ($\widehat{sec}$)	24

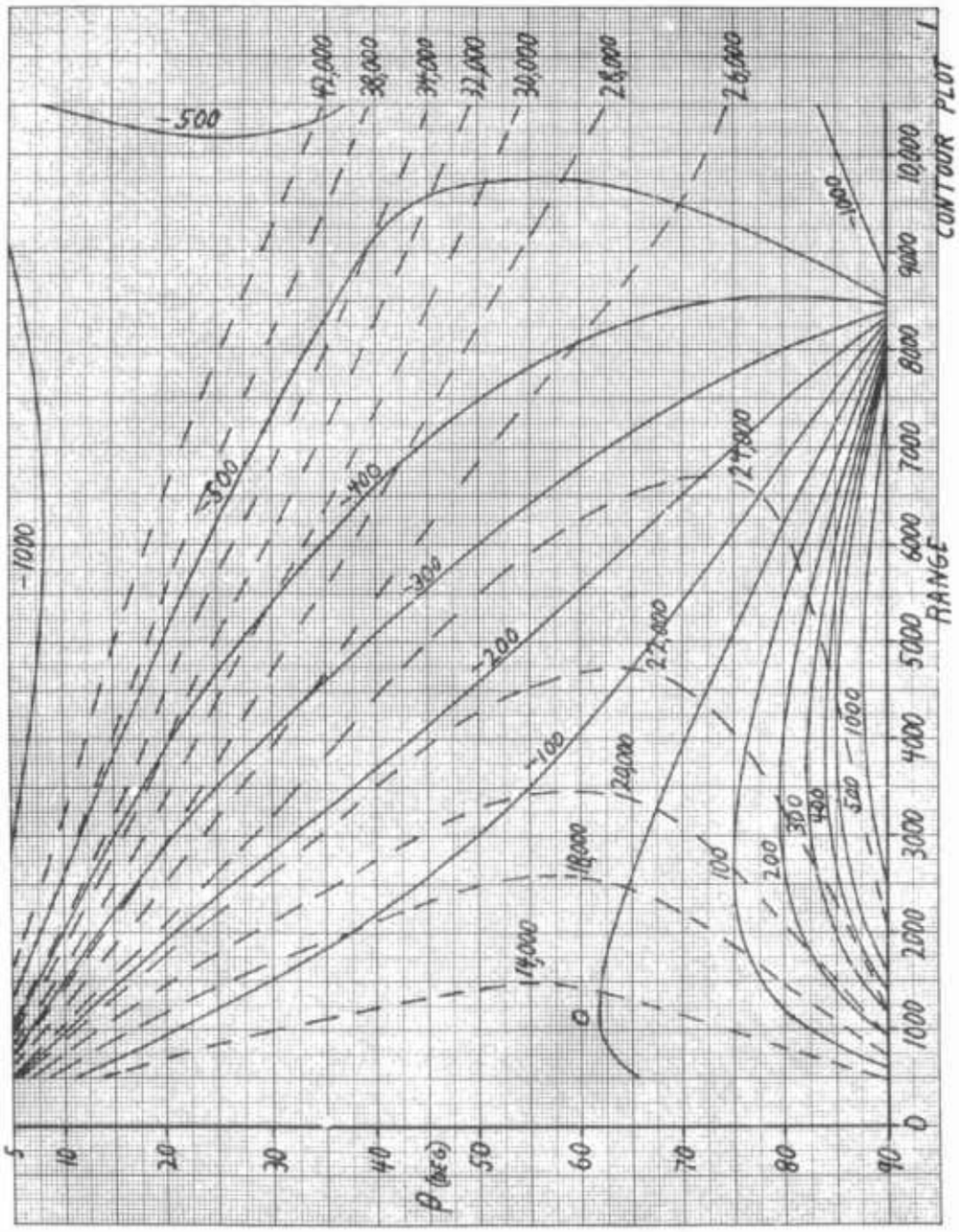
CONTOUR PLOT
RANGE
θ (DEG)
-500
-1000
-100
-200
-300
-400
40,000
38,000
34,000
32,000
30,000
28,000
26,000
24,000
22,000
20,000
18,000
16,000
14,000
12,000
10,000
8000
7000
6000
5000
4000
3000
2000
1000
0
100
200
300
400
500
1000
10
20
30
40
50
60
70
80
90

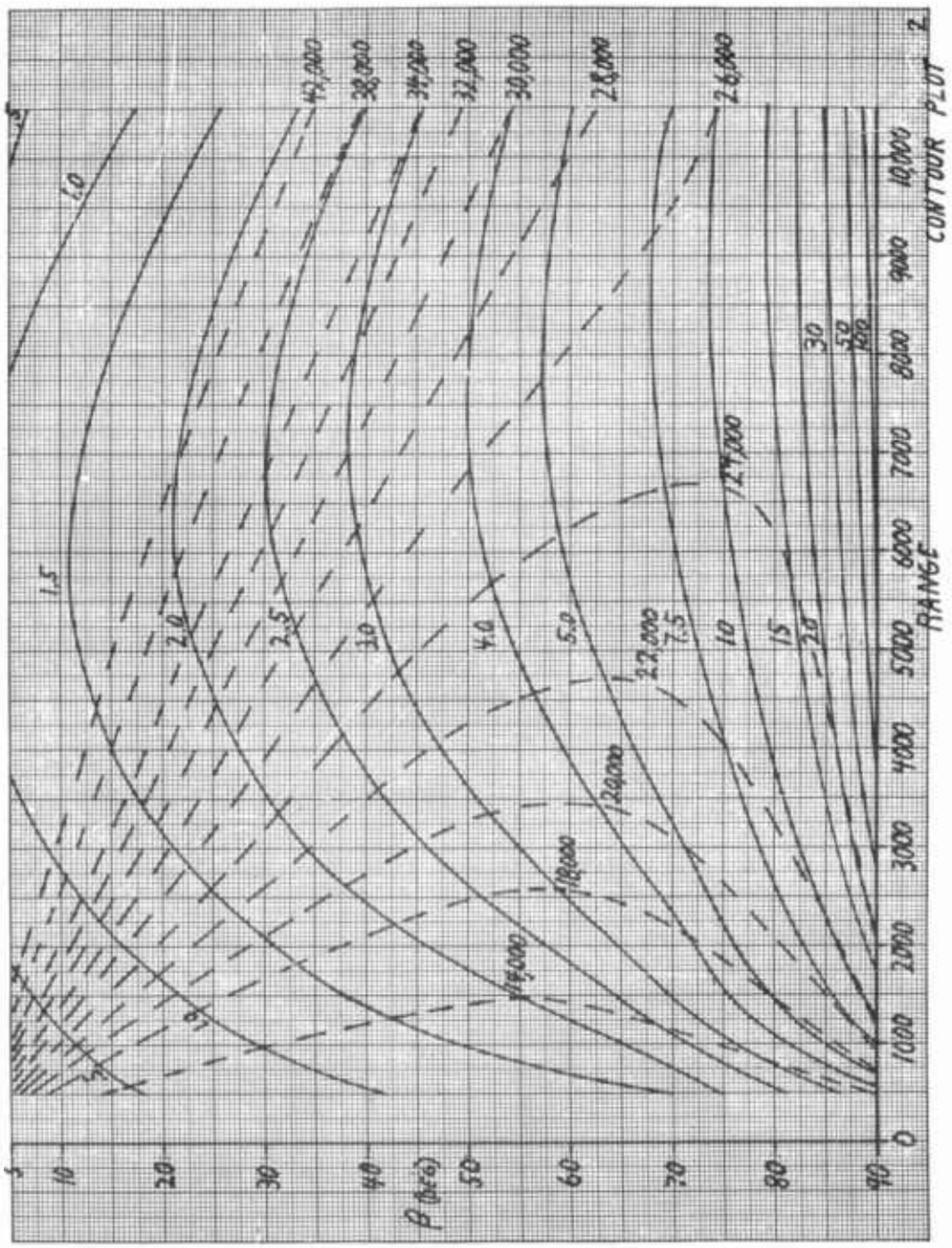
CONTOUR PLOT
RANGE
θ (DEG)
40,000
38,000
36,000
32,000
30,000
28,000
26,000
24,000
22,000
20,000
18,000
16,000
14,000
12,000
10,000
8000
7000
6000
5000
4000
3000
2000
1000
0
10
20
30
40
50
60
70
80
90
1.0
1.5
2.0
2.5
3.0
4.0
5.0
7.5
10
15
20
30
50
80

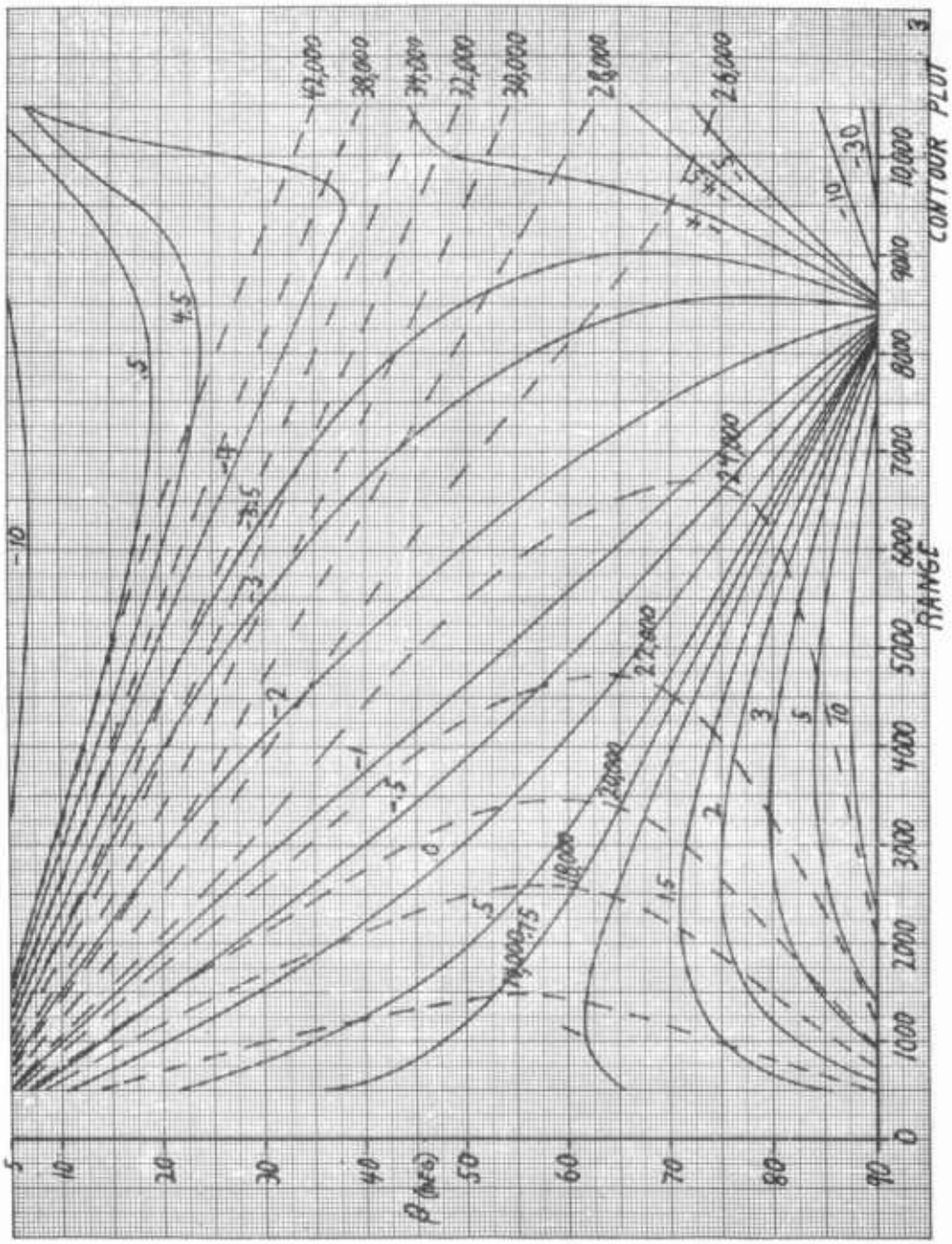
CONTOUR PLOT
RANGE
ρ (NMI)
43,000
38,000
34,000
30,000
26,000
22,000
18,000
14,000
10,000
6000
2000
0
1000
2000
3000
4000
5000
6000
7000
8000
9000
10000
-10
-5
0
5
10
15
20
25
30
35
40
45
50
55
60
65
70
75
80
85
90

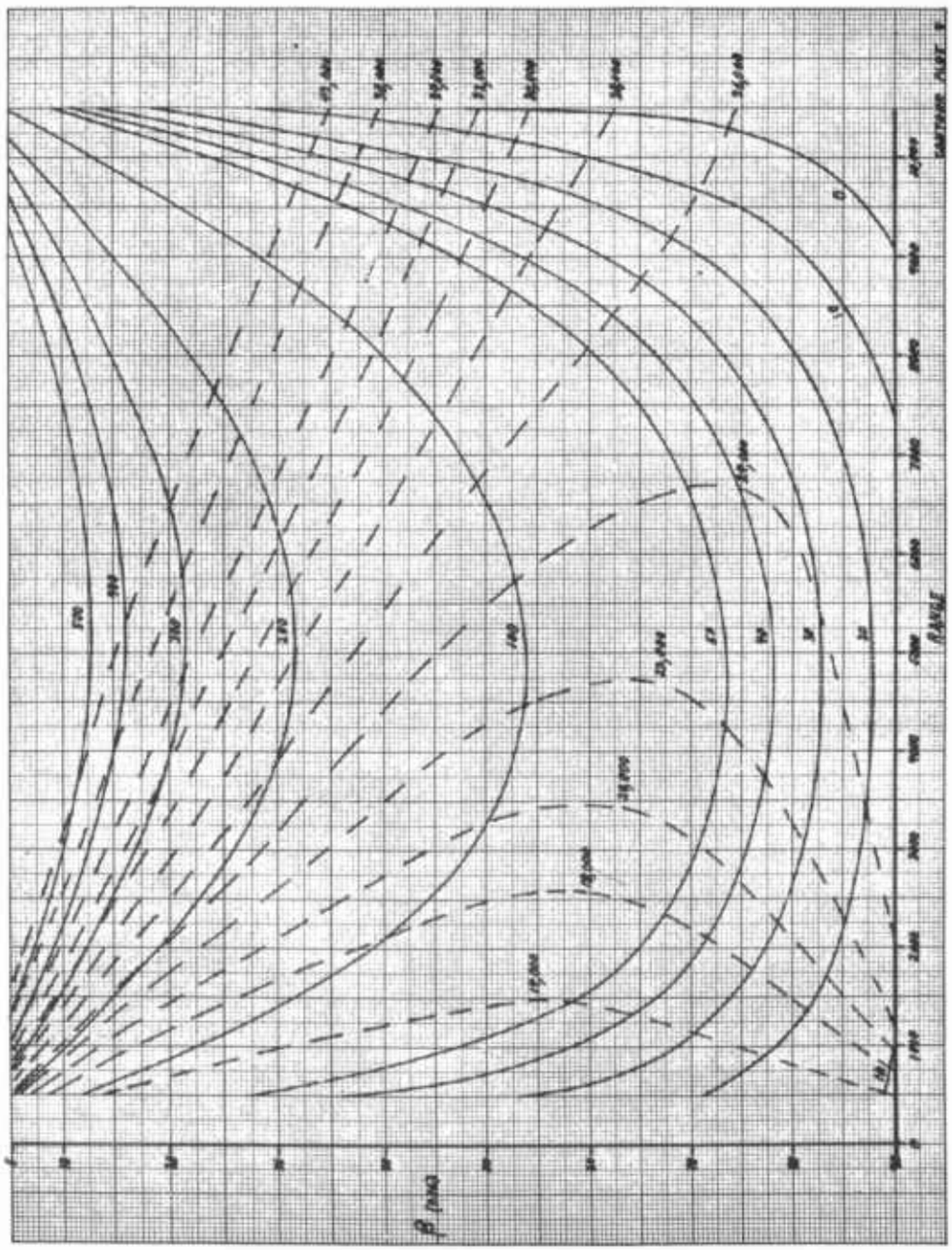

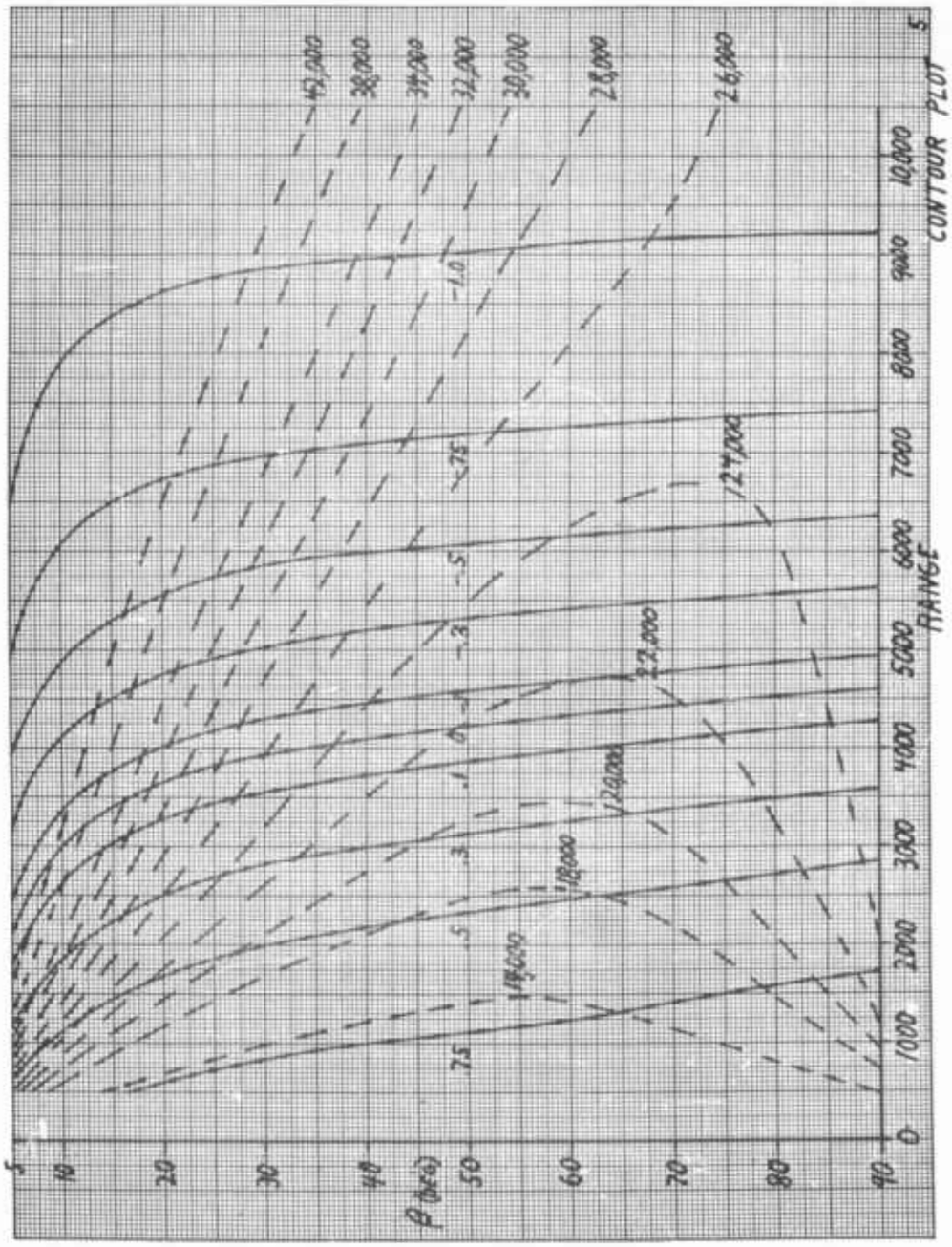
CONTOUR PLOT
RANGE
ALTITUDE
Q
M
40,000
38,000
36,000
34,000
32,000
30,000
28,000
26,000
24,000
22,000
20,000
18,000
16,000
14,000
12,000
10,000
8000
7000
6000
5000
4000
3000
2000
1000
-1.0
-.75
-.5
-.3
-.1
.1
.3
.5
.75
1.0
1.25
1.5
1.75
2.0
2.25
2.5
2.75
3.0
3.25
3.5
3.75
4.0
4.25
4.5
4.75
5.0
5.25
5.5
5.75
6.0
6.25
6.5
6.75
7.0
7.25
7.5
7.75
8.0
8.25
8.5
8.75
9.0
9.25
9.5
9.75
10.0
10.25
10.5
10.75
11.0
11.25
11.5
11.75
12.0
12.25
12.5
12.75
13.0
13.25
13.5
13.75
14.0
14.25
14.5
14.75
15.0
15.25
15.5
15.75
16.0
16.25
16.5
16.75
17.0
17.25
17.5
17.75
18.0
18.25
18.5
18.75
19.0
19.25
19.5
19.75
20.0

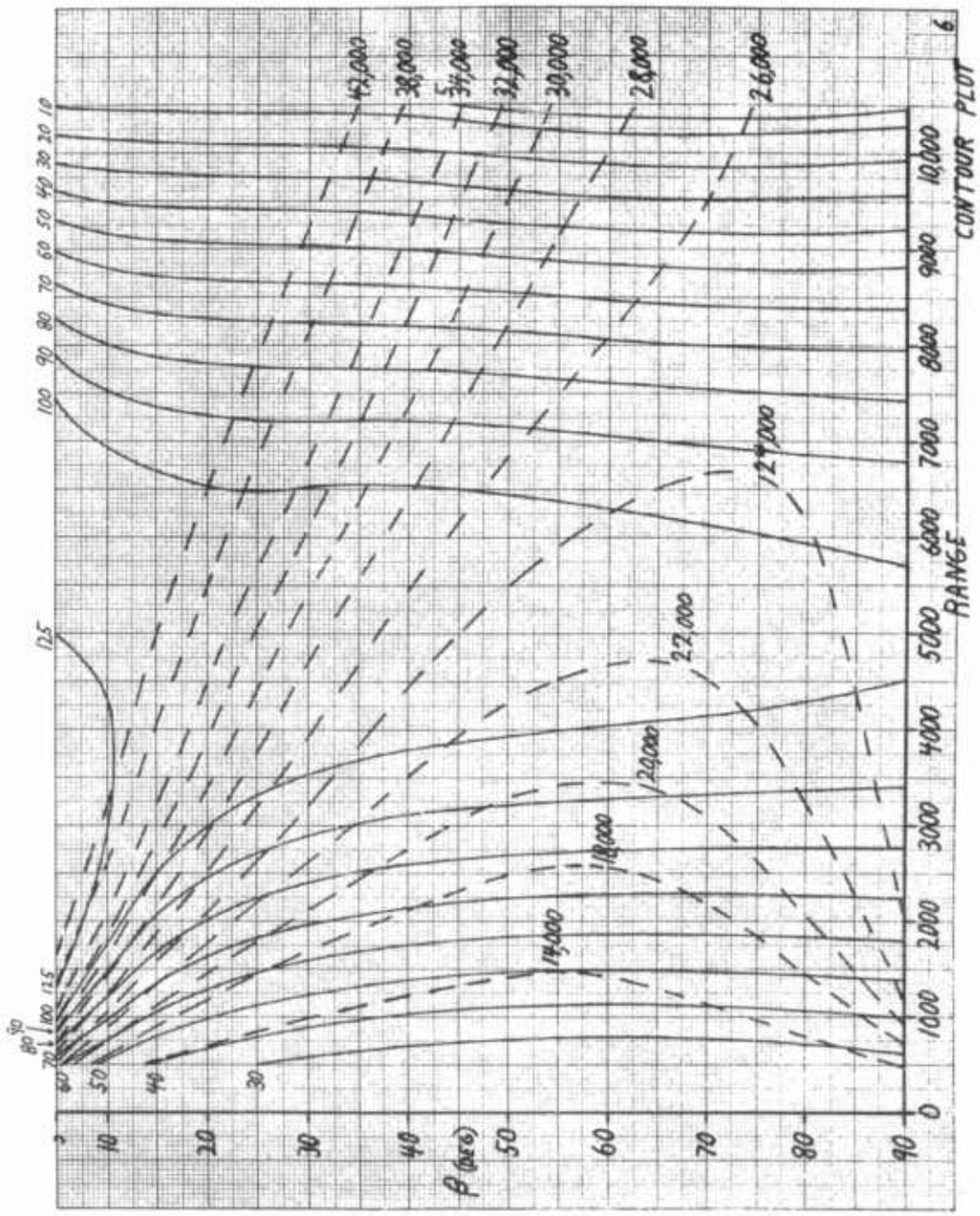
CONTOUR PLOT
RANGE
ρ (DEG)
42,000
38,000
34,000
32,000
30,000
28,000
26,000
22,000
18,000
14,000

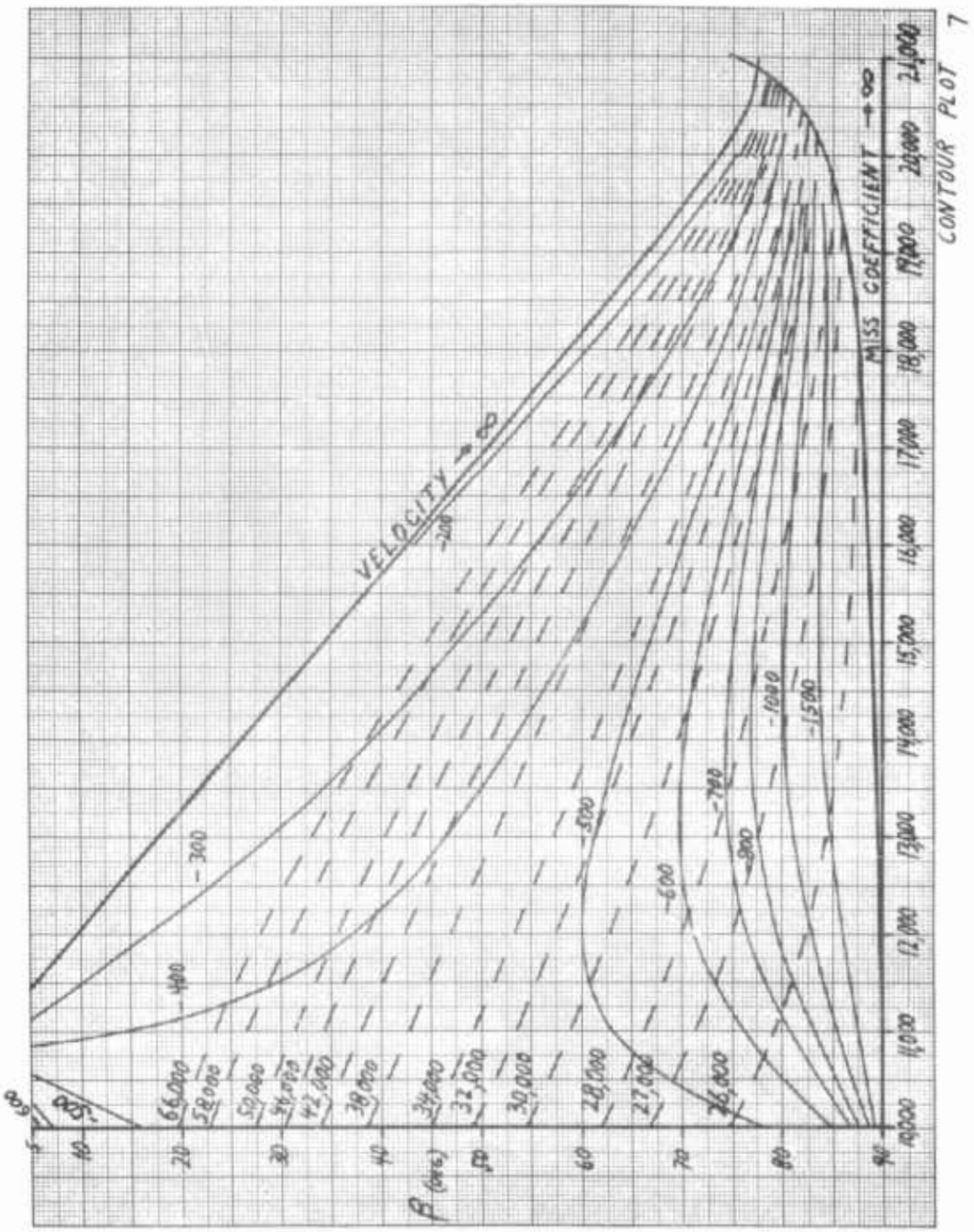
CONTOUR PLOT 7
MISS COEFFICIENT → ∞
VELOCITY → ∞
-200
-300
-400
-500
-600
-700
-800
-900
-1000
-1500
66,000
58,000
50,000
42,000
38,000
34,000
32,000
30,000
28,000
27,000
26,400
β (deg.)
ALTITUDE (ft)

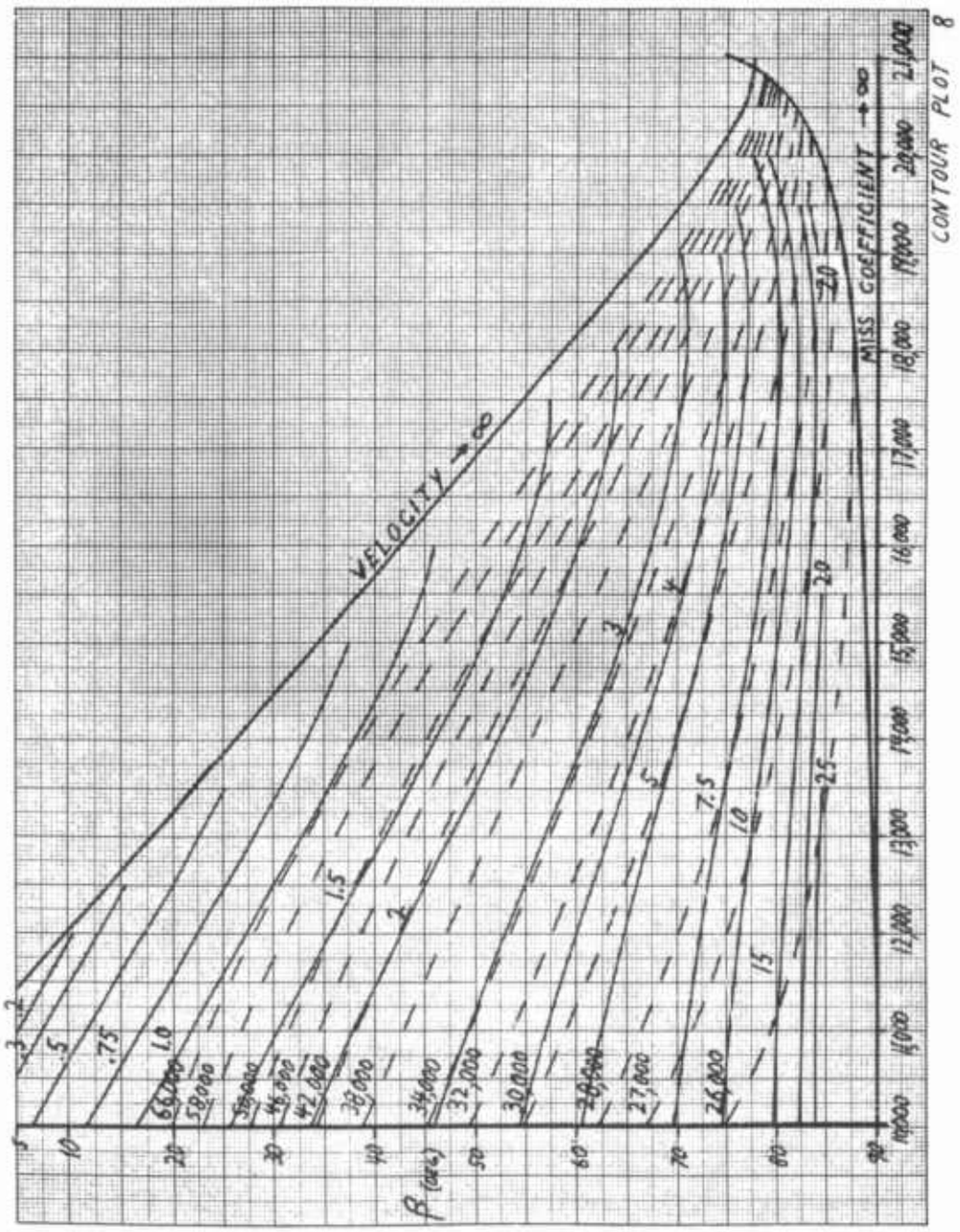
CONTOUR PLOT 8
MISS COEFFICIENT → ∞
VELOCITY → ∞
β (deg.)
5
10
20
30
40
50
60
70
80
90
68,000
58,000
50,000
46,000
42,000
38,000
34,000
32,000
30,000
28,000
27,000
26,000
.3
.5
.75
1.0
1.5
2
3
5
7.5
10
15
20
25

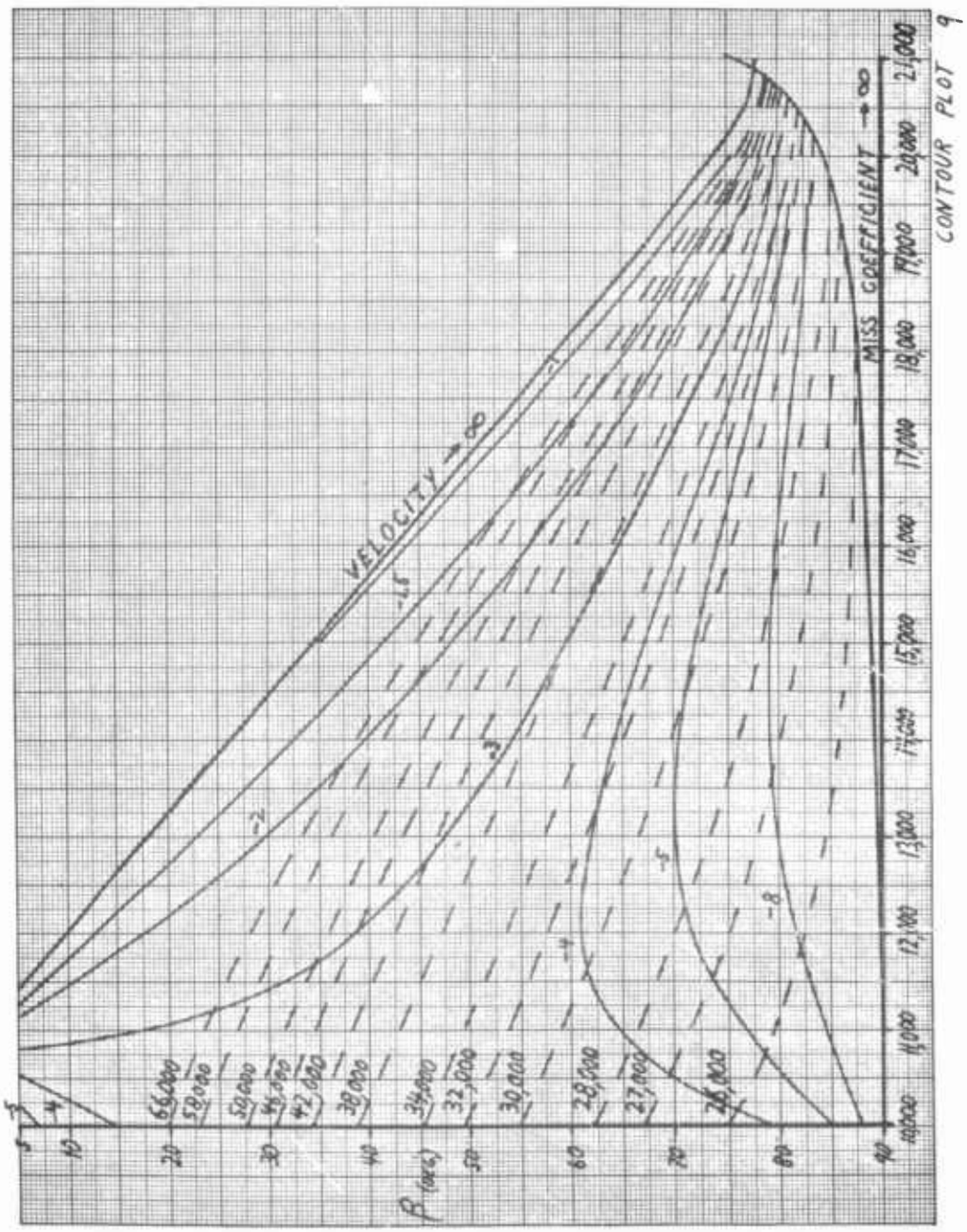
CONTOUR PLOT 9
MISS COEFFICIENT → ∞
VELOCITY → ∞
-1
-.5
-.3
-2
-4
-5
-8
-10
-15
-20
66,000
58,000
50,000
46,000
42,000
38,000
34,000
32,000
30,000
28,000
27,000
26,000
21,000
20,000
19,000
18,000
17,000
16,000
15,000
14,000
13,000
12,000
11,000
10,000
9,000
8,000
7,000
6,000
5,000
4,000
3,000
2,000
1,000
R (NAUT)

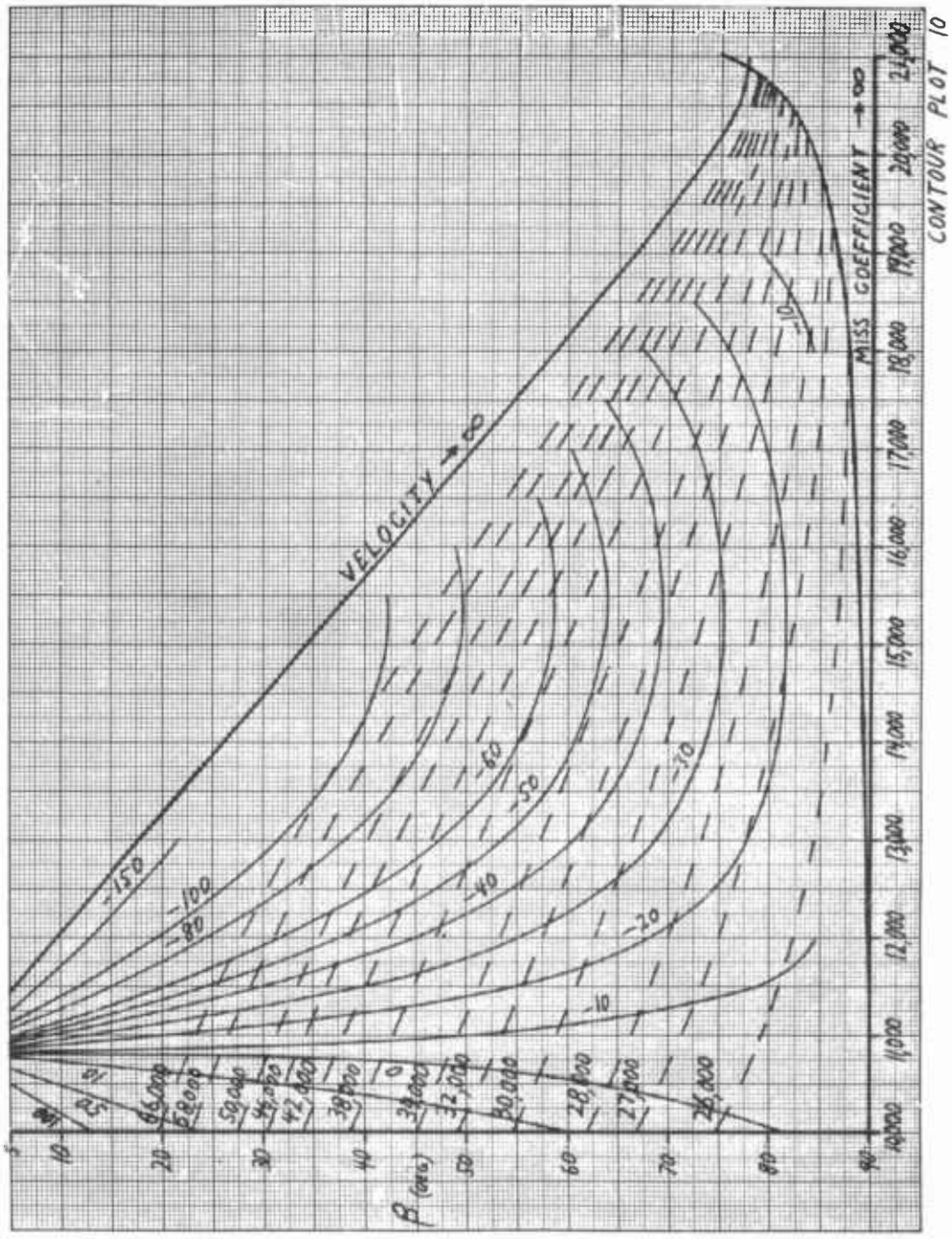
CONTOUR PLOT 10
MISS COEFFICIENT → ∞
VELOCITY → ∞
-150
-100
-90
-60
-50
-40
-30
-20
-10
β (DEG.)

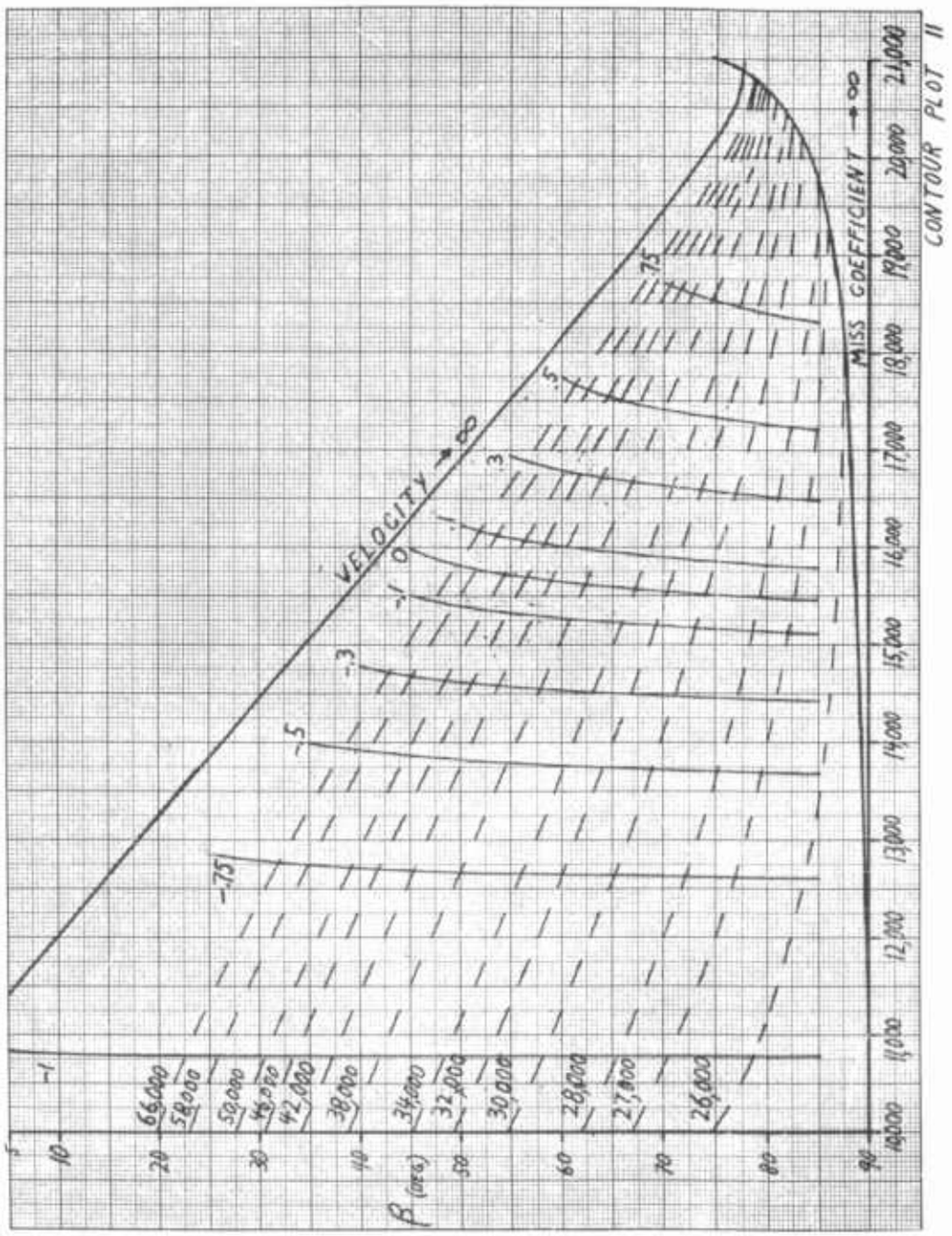
CONTOUR PLOT II
MISS COEFFICIENT → ∞
VELOCITY → ∞
-1
-.75
-.5
-.3
-.1
0
.3
.5
.75
1
β (deg.)
5
10
20
30
40
50
60
70
80
90
66,000
58,000
50,000
46,000
42,000
38,000
34,000
32,000
30,000
28,000
27,000
26,000
21,000
20,000
19,000
18,000
17,000
16,000
15,000
14,000
13,000
12,000
11,000
10,000

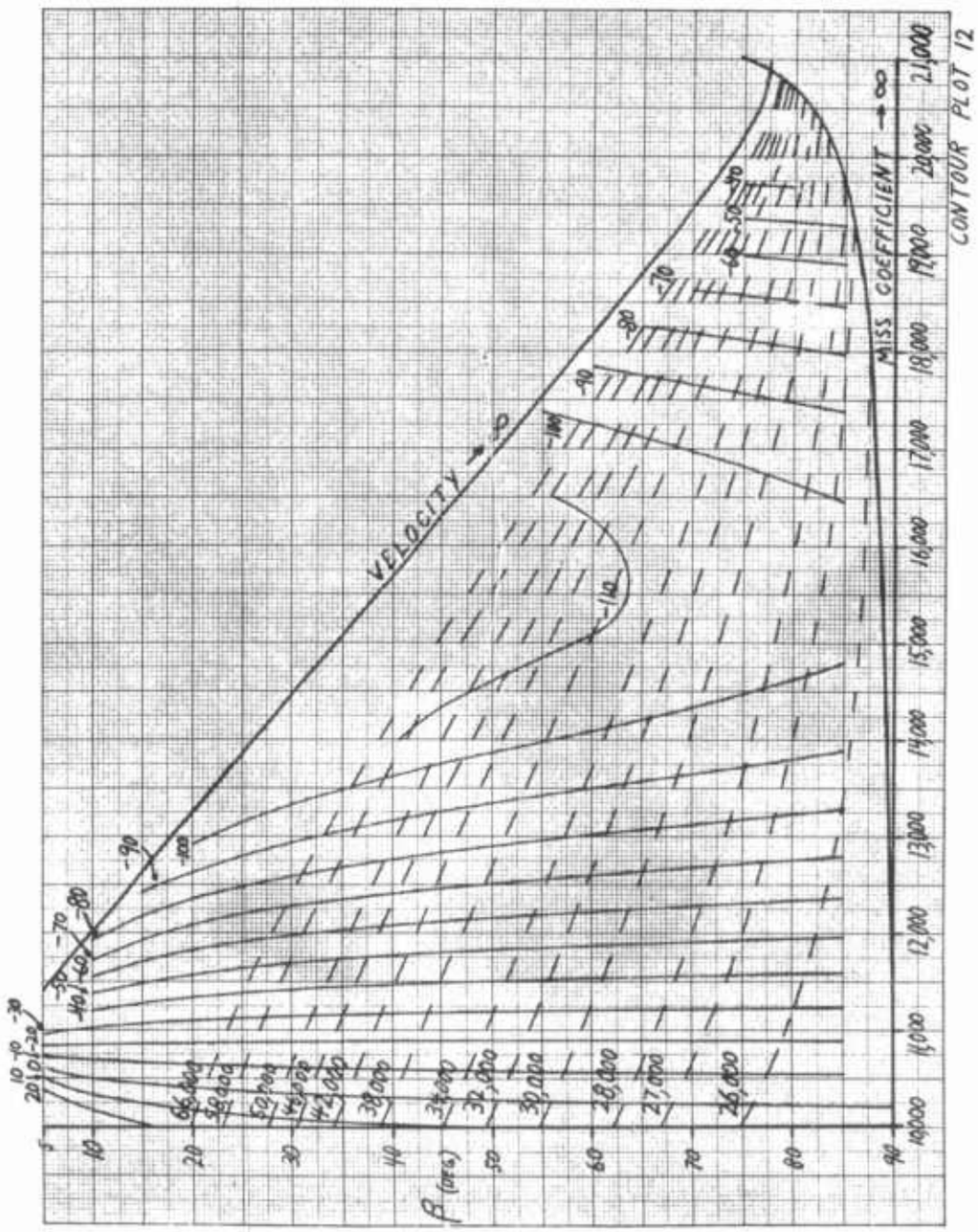
CONTOUR PLOT 12
MASS COEFFICIENT → ∞
VELOCITY → 0
R (ohms)

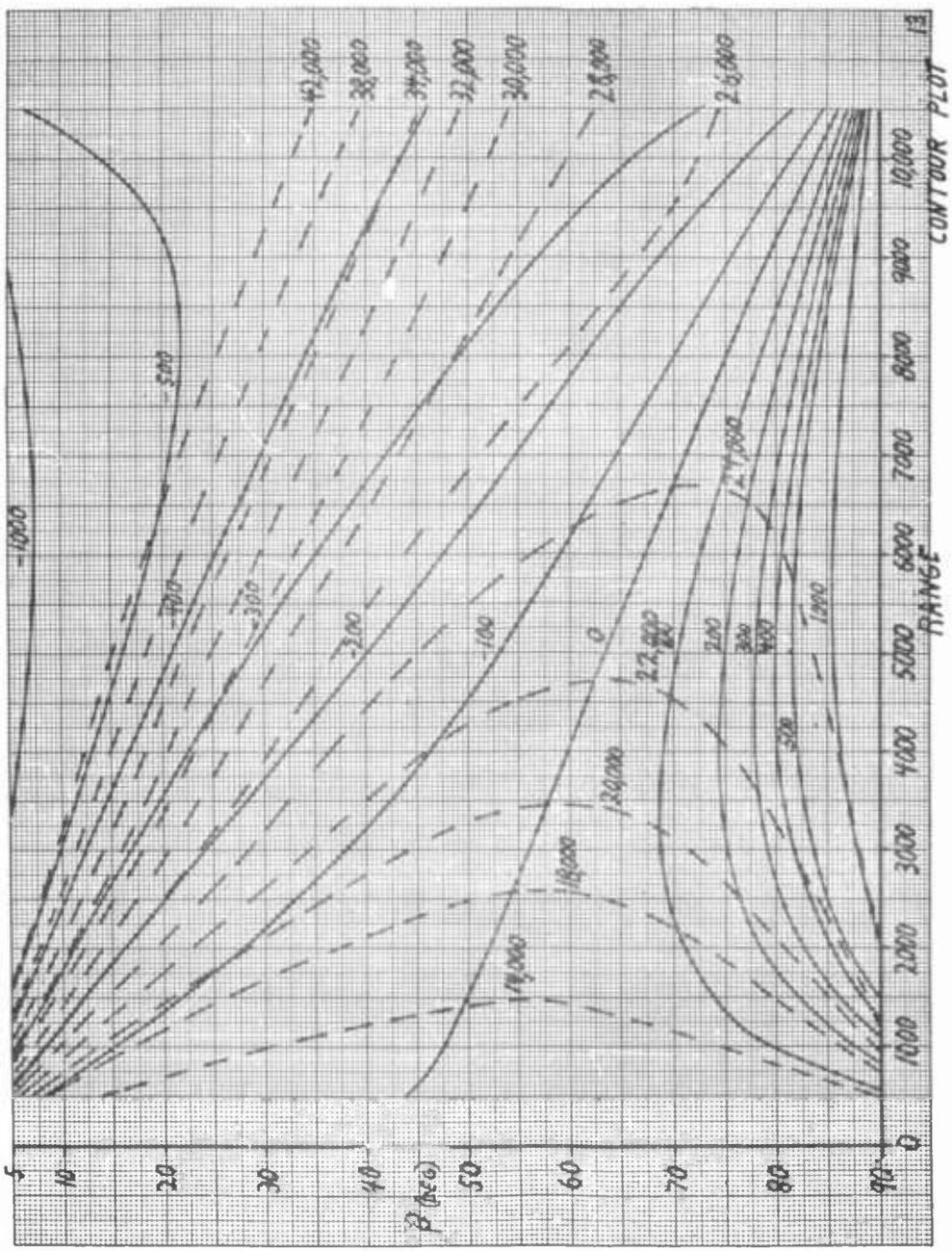
CONTOUR PLOT
RANGE
ft
0
1000
2000
3000
4000
5000
6000
7000
8000
10000
26,000
28,000
30,000
32,000
34,000
38,000
42,000
-500
-1000
-400
-300
-200
-100
0
100
200
300
400
500
1000
1,000
2,000
3,000
4,000
5,000
6,000
7,000
8,000
10,000
12,000
14,000
16,000
18,000
20,000
22,000
24,000
26,000
28,000
30,000
32,000
34,000
36,000
38,000
40,000
42,000
44,000
46,000
48,000
50,000
52,000
54,000
56,000
58,000
60,000
62,000
64,000
66,000
68,000
70,000
72,000
74,000
76,000
78,000
80,000
82,000
84,000
86,000
88,000
90,000
92,000
94,000
96,000
98,000
100,000
102,000
104,000
106,000
108,000
110,000
112,000
114,000
116,000
118,000
120,000
122,000
124,000
126,000
128,000
130,000
132,000
134,000
136,000
138,000
140,000
142,000
144,000
146,000
148,000
150,000
152,000
154,000
156,000
158,000
160,000
162,000
164,000
166,000
168,000
170,000
172,000
174,000
176,000
178,000
180,000
182,000
184,000
186,000
188,000
190,000
192,000
194,000
196,000
198,000
200,000
202,000
204,000
206,000
208,000
210,000
212,000
214,000
216,000
218,000
220,000
222,000
224,000
226,000
228,000
230,000
232,000
234,000
236,000
238,000
240,000
242,000
244,000
246,000
248,000
250,000
252,000
254,000
256,000
258,000
260,000
262,000
264,000
266,000
268,000
270,000
272,000
274,000
276,000
278,000
280,000
282,000
284,000
286,000
288,000
290,000
292,000
294,000
296,000
298,000
300,000
302,000
304,000
306,000
308,000
310,000
312,000
314,000
316,000
318,000
320,000
322,000
324,000
326,000
328,000
330,000
332,000
334,000
336,000
338,000
340,000
342,000
344,000
346,000
348,000
350,000
352,000
354,000
356,000
358,000
360,000
362,000
364,000
366,000
368,000
370,000
372,000
374,000
376,000
378,000
380,000
382,000
384,000
386,000
388,000
390,000
392,000
394,000
396,000
398,000
400,000
402,000
404,000
406,000
408,000
410,000
412,000
414,000
416,000
418,000
420,000
422,000
424,000
426,000
428,000
430,000
432,000
434,000
436,000
438,000
440,000
442,000
444,000
446,000
448,000
450,000
452,000
454,000
456,000
458,000
460,000
462,000
464,000
466,000
468,000
470,000
472,000
474,000
476,000
478,000
480,000
482,000
484,000
486,000
488,000
490,000
492,000
494,000
496,000
498,000
500,000
502,000
504,000
506,000
508,000
510,000
512,000
514,000
516,000
518,000
520,000
522,000
524,000
526,000
528,000
530,000
532,000
534,000
536,000
538,000
540,000
542,000
544,000
546,000
548,000
550,000
552,000
554,000
556,000
558,000
560,000
562,000
564,000
566,000
568,000
570,000
572,000
574,000
576,000
578,000
580,000
582,000
584,000
586,000
588,000
590,000
592,000
594,000
596,000
598,000
600,000
602,000
604,000
606,000
608,000
610,000
612,000
614,000
616,000
618,000
620,000
622,000
624,000
626,000
628,000
630,000
632,000
634,000
636,000
638,000
640,000
642,000
644,000
646,000
648,000
650,000
652,000
654,000
656,000
658,000
660,000
662,000
664,000
666,000
668,000
670,000
672,000
674,000
676,000
678,000
680,000
682,000
684,000
686,000
688,000
690,000
692,000
694,000
696,000
698,000
700,000
702,000
704,000
706,000
708,000
710,000
712,000
714,000
716,000
718,000
720,000
722,000
724,000
726,000
728,000
730,000
732,000
734,000
736,000
738,000
740,000
742,000
744,000
746,000
748,000
750,000
752,000
754,000
756,000
758,000
760,000
762,000
764,000
766,000
768,000
770,000
772,000
774,000
776,000
778,000
780,000
782,000
784,000
786,000
788,000
790,000
792,000
794,000
796,000
798,000
800,000
802,000
804,000
806,000
808,000
810,000
812,000
814,000
816,000
818,000
820,000
822,000
824,000
826,000
828,000
830,000
832,000
834,000
836,000
838,000
840,000
842,000
844,000
846,000
848,000
850,000
852,000
854,000
856,000
858,000
860,000
862,000
864,000
866,000
868,000
870,000
872,000
874,000
876,000
878,000
880,000
882,000
884,000
886,000
888,000
890,000
892,000
894,000
896,000
898,000
900,000
902,000
904,000
906,000
908,000
910,000
912,000
914,000
916,000
918,000
920,000
922,000
924,000
926,000
928,000
930,000
932,000
934,000
936,000
938,000
940,000
942,000
944,000
946,000
948,000
950,000
952,000
954,000
956,000
958,000
960,000
962,000
964,000
966,000
968,000
970,000
972,000
974,000
976,000
978,000
980,000
982,000
984,000
986,000
988,000
990,000
992,000
994,000
996,000
998,000
1000,000

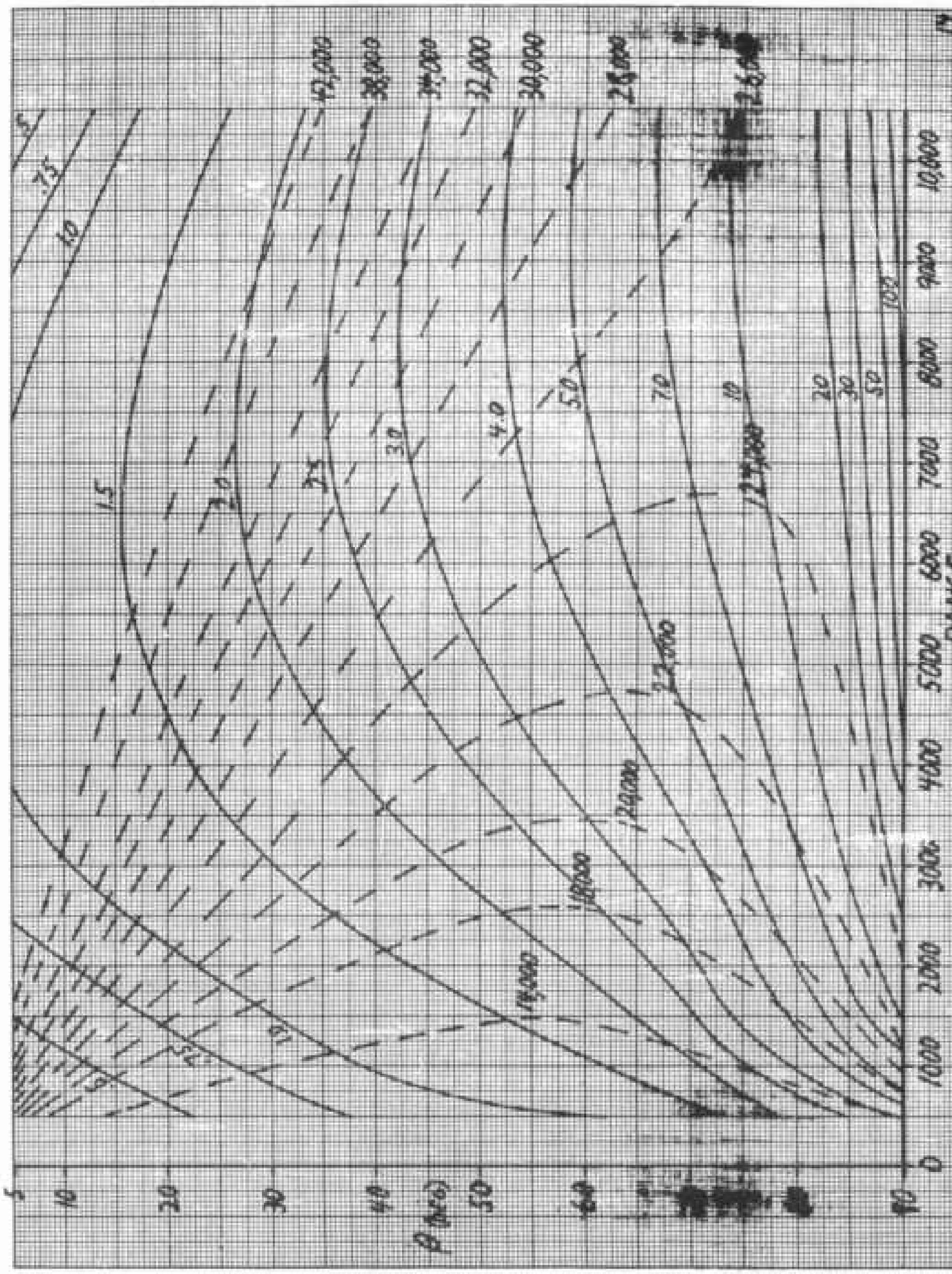
CONTOUR PLOT
RANGE
β (deg)

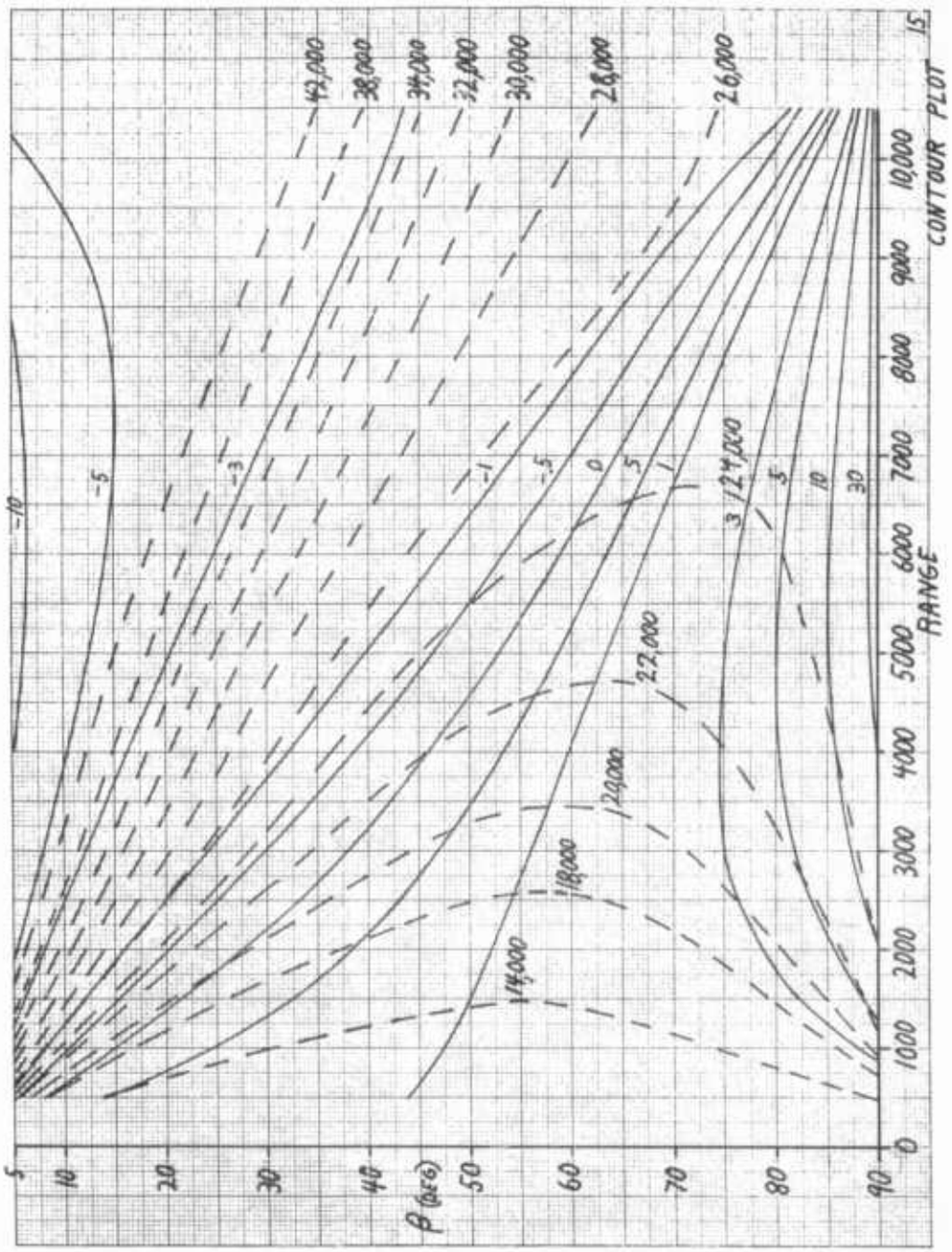
CONTOUR PLOT
RANGE
β (DEG)
42,000
38,000
34,000
32,000
30,000
28,000
26,000
-10
-5
-3
-1
-.5
0
.5
1
3
5
10
30
14,000
18,000
24,000
27,000
5
10
20
30
40
50
60
70
80
90
0
1000
2000
3000
4000
5000
6000
7000
8000
9000
10,000

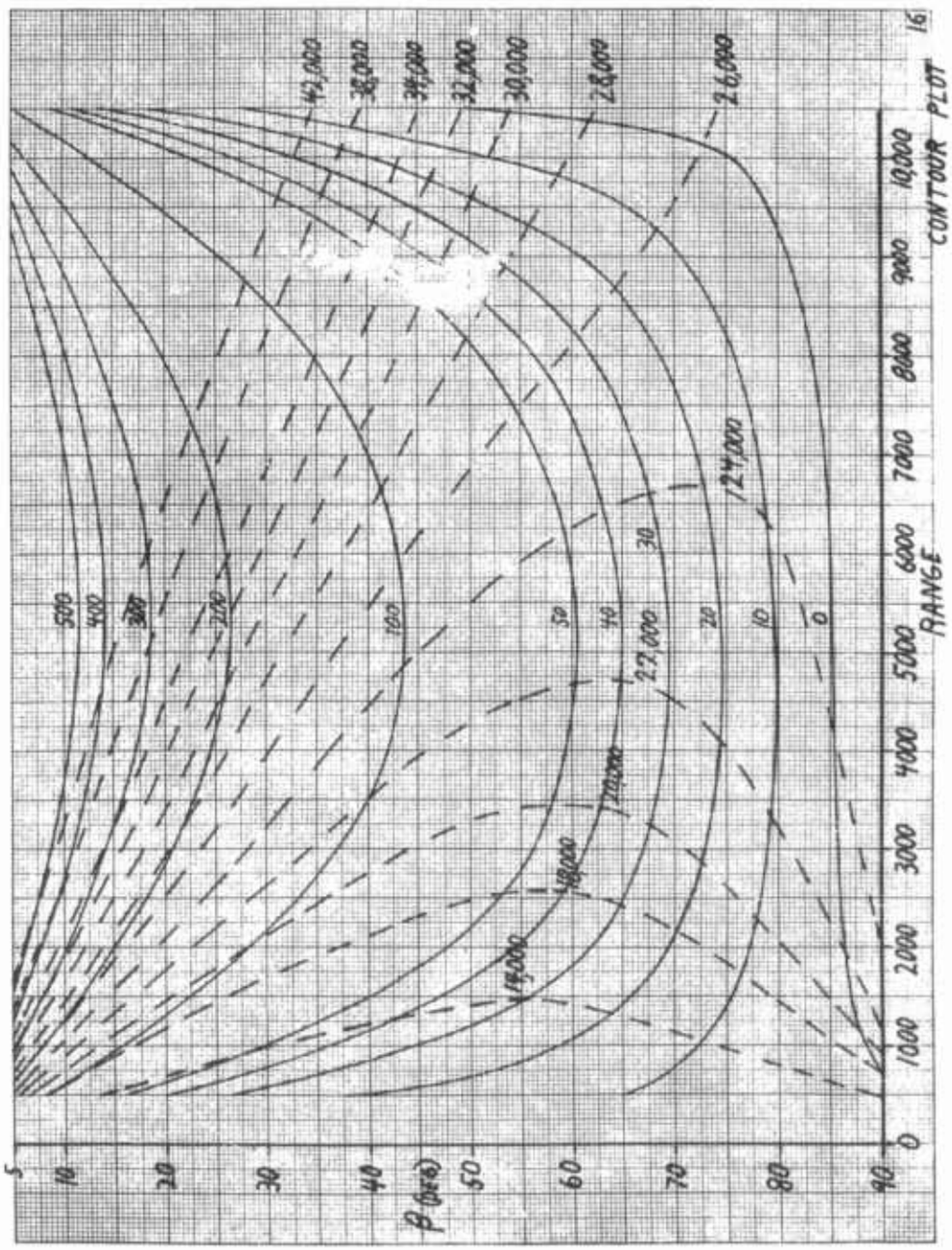
CONTOUR PLOT
RANGE
θ (deg)
0
1000
2000
3000
4000
5000
6000
7000
8000
9000
10000
0
10
20
30
40
50
60
70
80
90
500
400
300
200
100
0
10
20
30
40
50
60
70
80
90
24,000
27,000
30,000
33,000
36,000
39,000
42,000
45,000
48,000
51,000
54,000

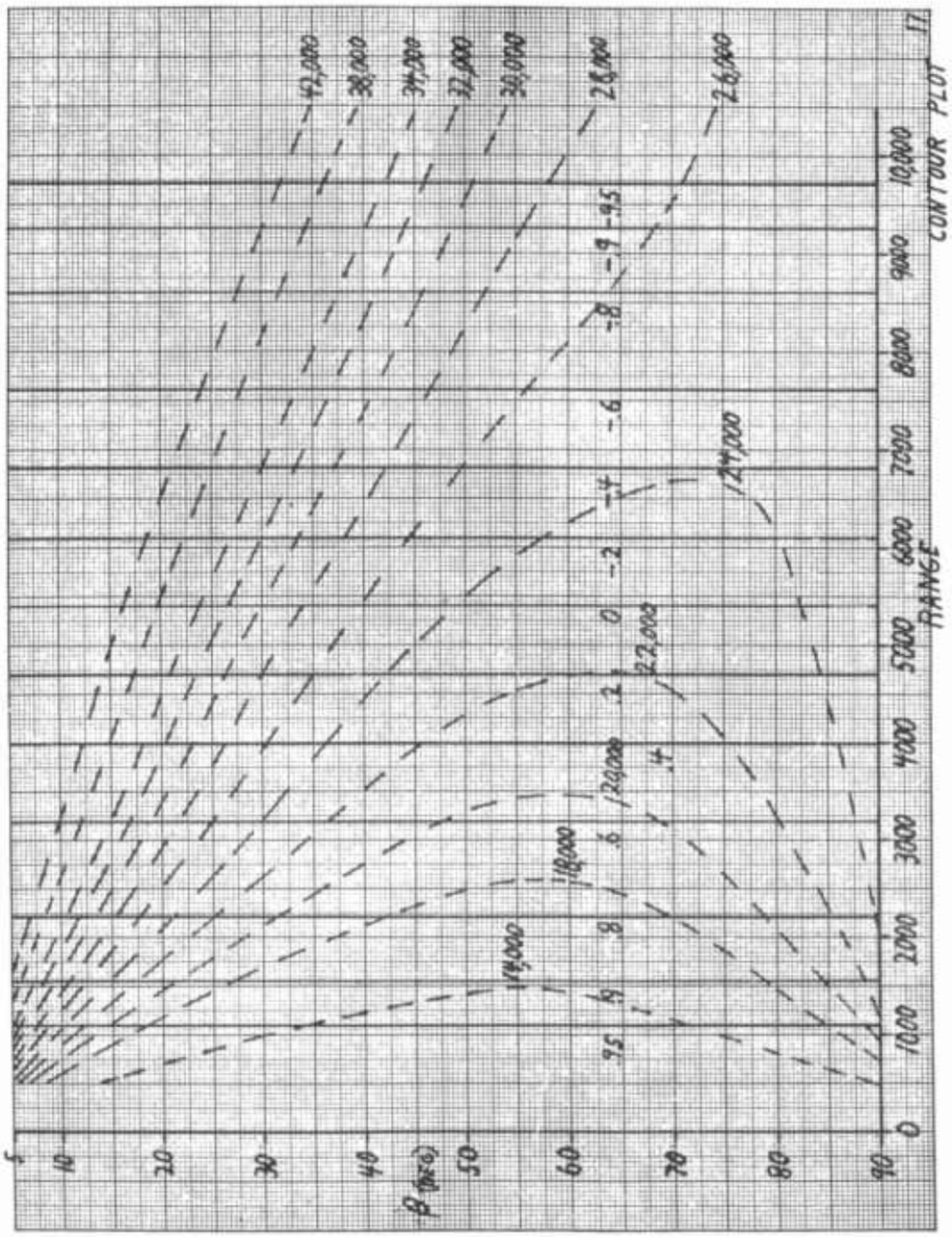
CONTOUR PLOT
RANGE
0
1000
2000
3000
4000
5000
6000
7000
8000
9000
10,000
-26,000
-28,000
-30,000
-32,000
-34,000
-36,000
-38,000
-40,000
-9.5
-9
-8
-6
-4
-2
0
2
4
6
8
9
9.5
22,000
24,000
120,000
140,000
160,000
β (DEG)
5
10
20
30
40
50
60
70
80
90

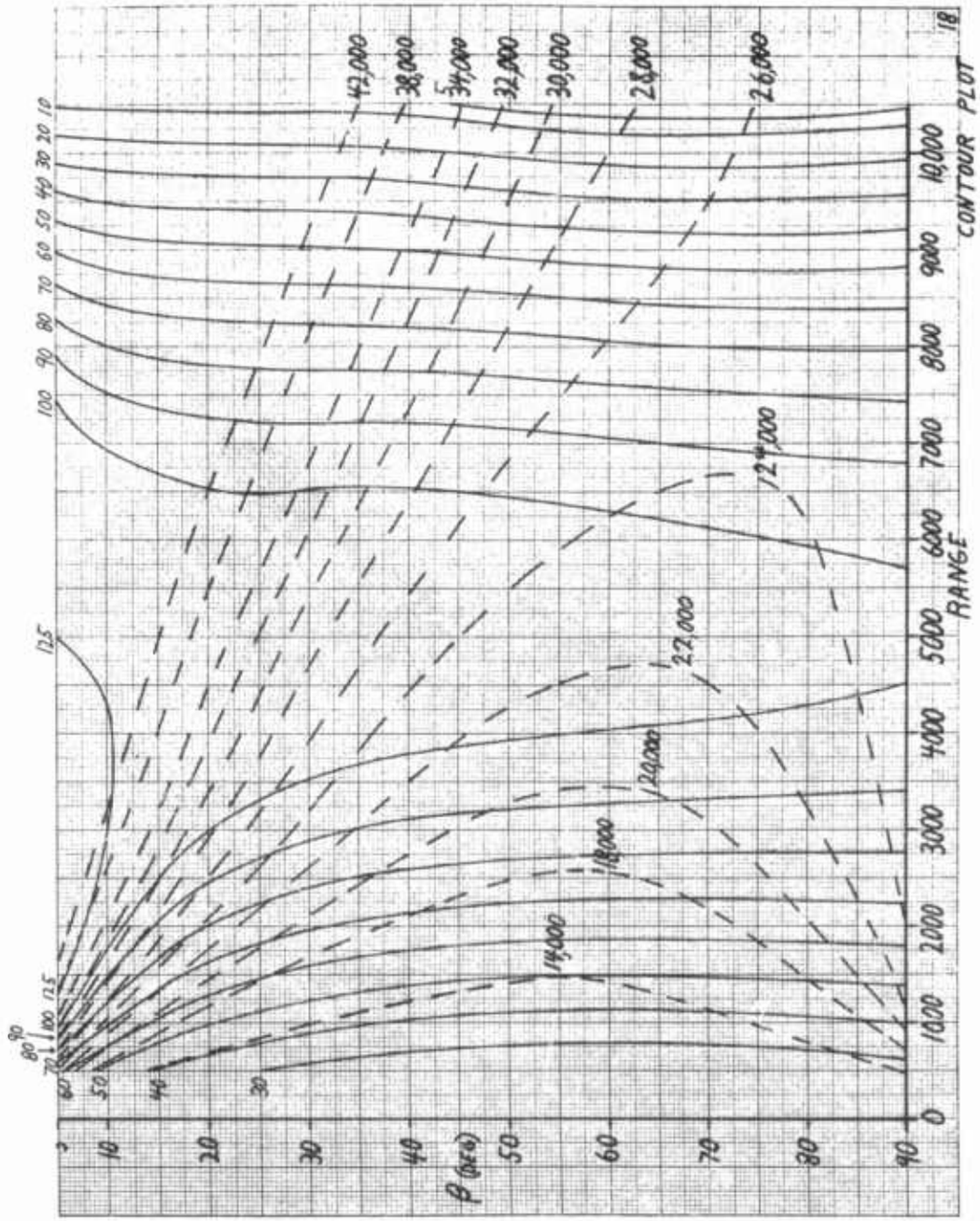
CONTOUR PLOT
RANGE
θ (deg)
42,000
38,000
34,000
32,000
30,000
28,000
26,000
22,000
18,000
14,000
10,000
0
1000
2000
3000
4000
5000
6000
7000
8000
9000
10000

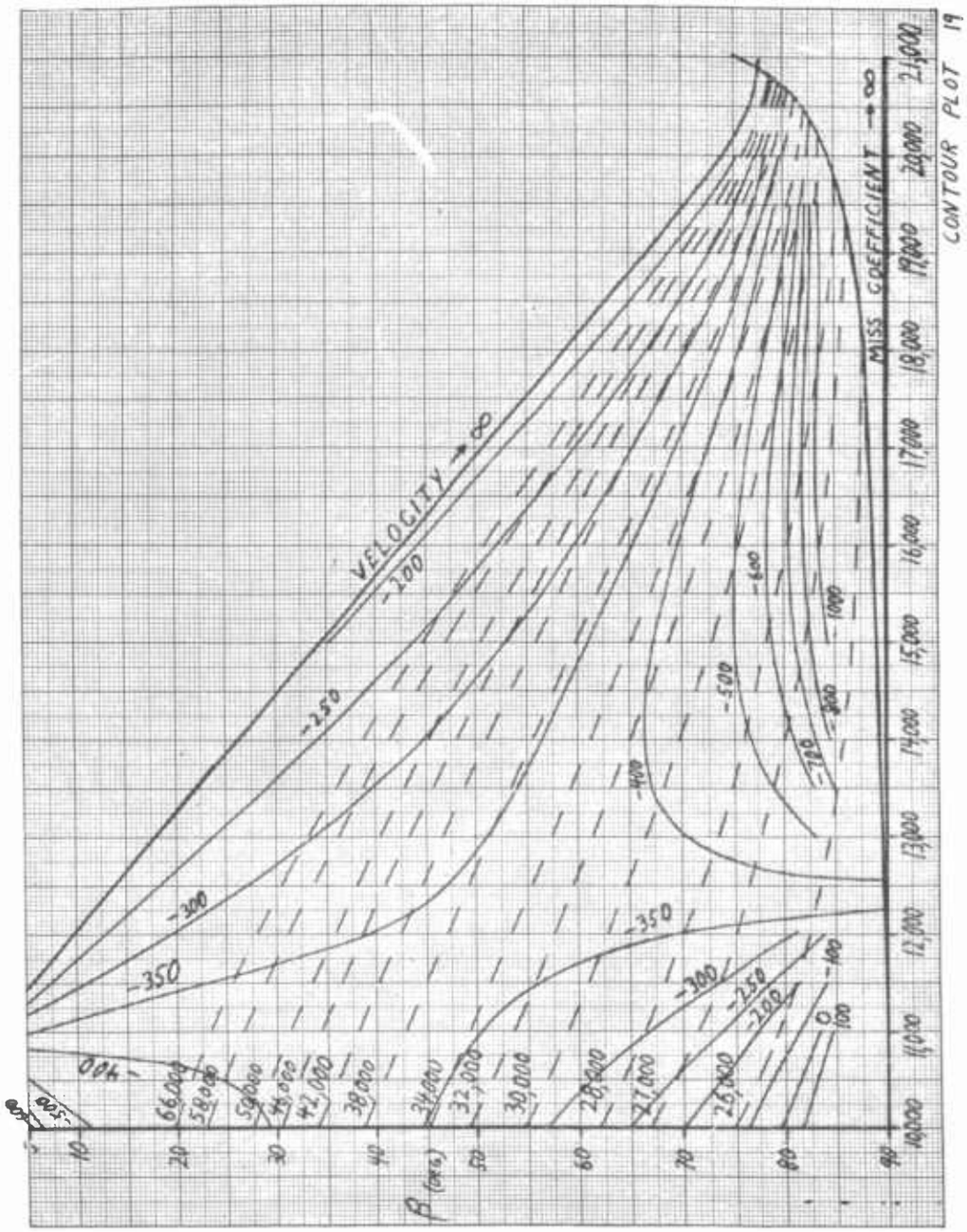
CONTOUR PLOT 19
MISS COEFFICIENT → ∞
VELOCITY → ∞
-100
-150
-200
-250
-300
-350
-400
-500
-600
-700
-800
-1000
0
100
B (DEG.)
10
20
30
40
50
60
70
80
90
66,000
58,000
50,000
46,000
42,000
38,000
34,000
32,000
30,000
28,000
27,000
26,000
25,000
24,000
23,000
22,000
21,000
20,000
19,000
18,000
17,000
16,000
15,000
14,000
13,000
12,000
11,000
10,000

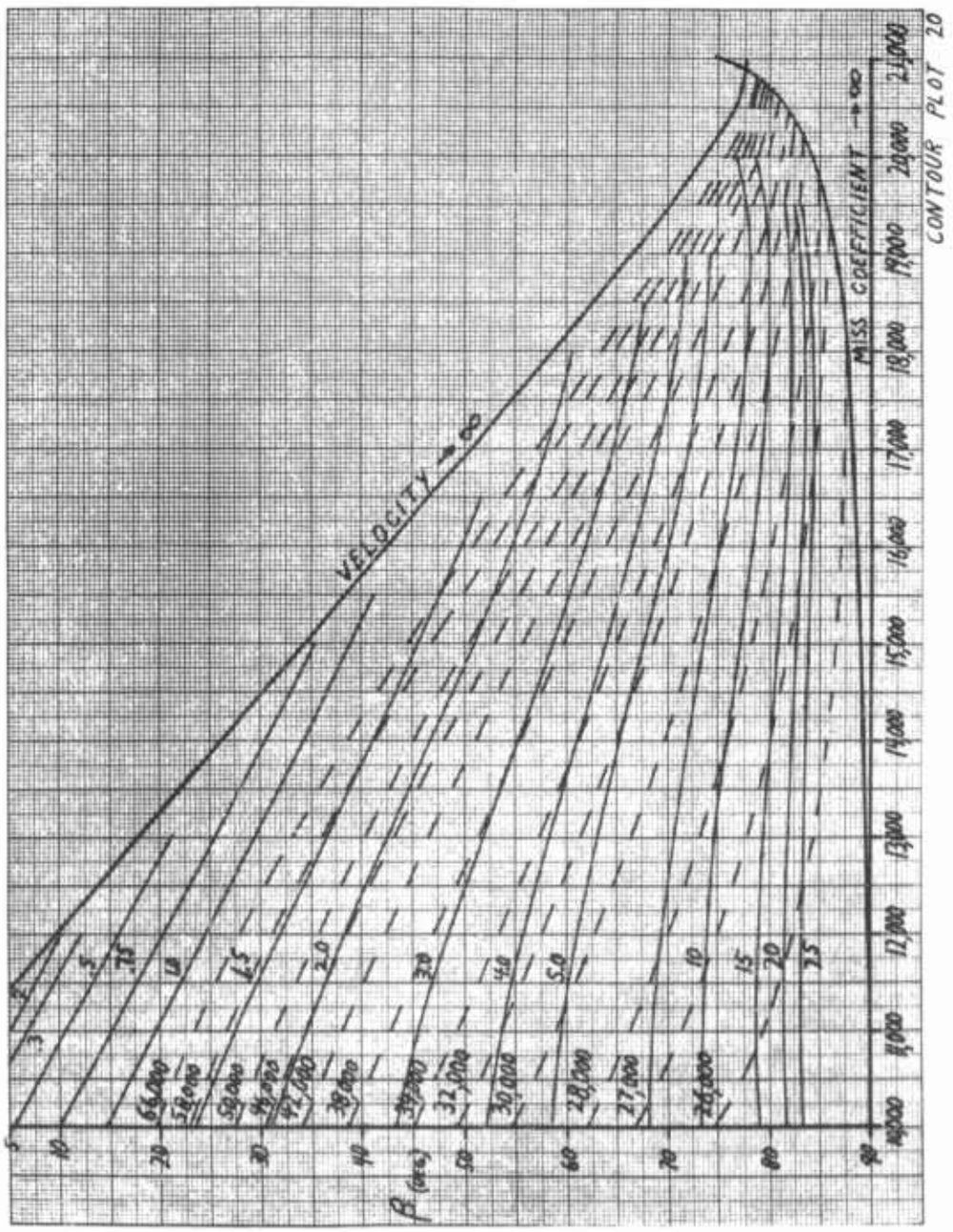
CONTOUR PLOT 20
MISS COEFFICIENT → ∞
VELOCITY → ∞
β (deg.)

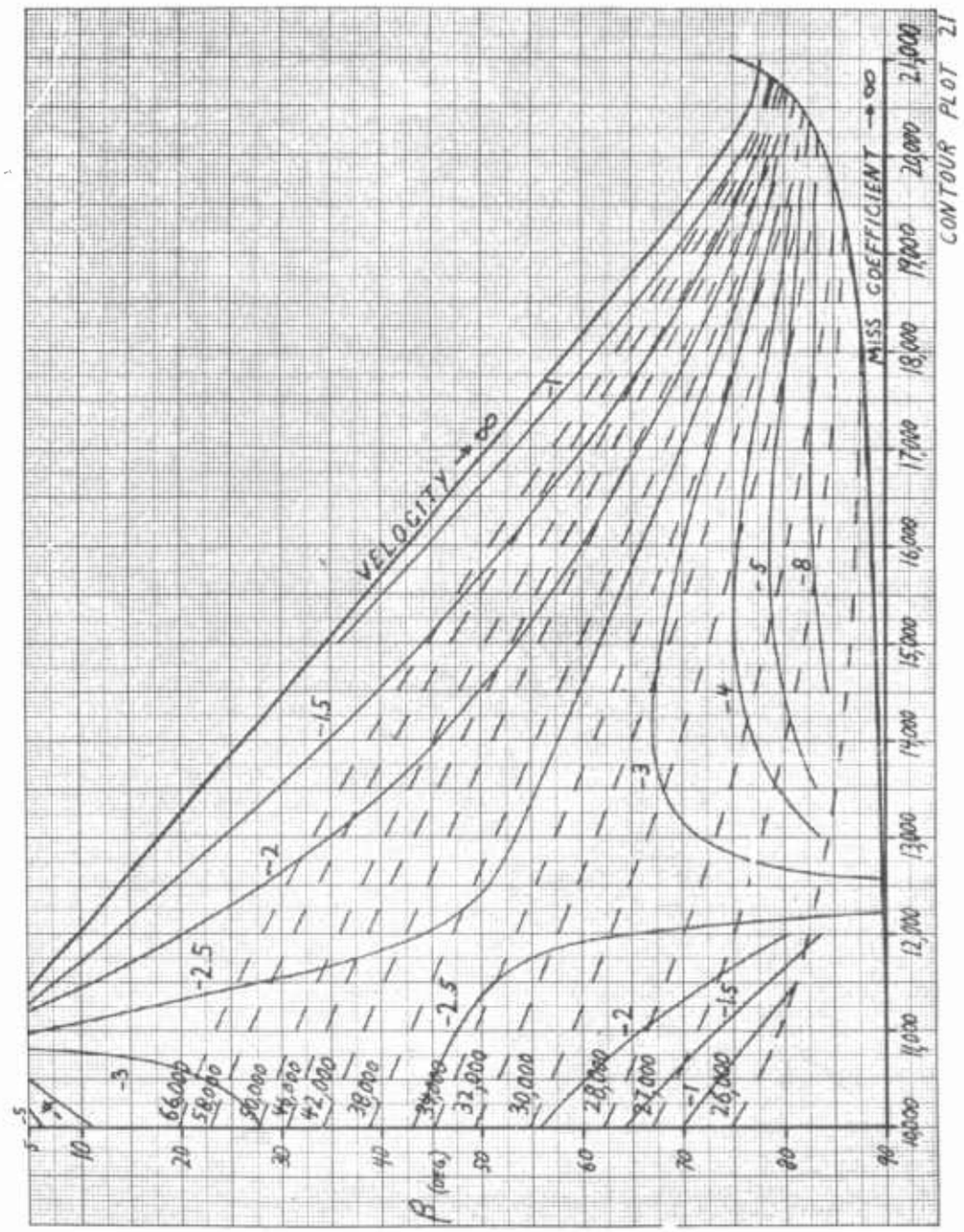
CONTOUR PLOT 21
MISS COEFFICIENT → ∞
VELOCITY → ∞
-1
-1.5
-2
-2.5
-3
-4
-5
-8
-2.5
-2
-1.5
-1
-3
-5
66,000
58,000
46,000
42,000
38,000
34,000
32,000
30,000
28,000
26,000
21,000
20,000
19,000
18,000
17,000
16,000
15,000
14,000
13,000
12,000
11,000
10,000
10
20
30
40
50
60
70
80
90
β (DEG.)

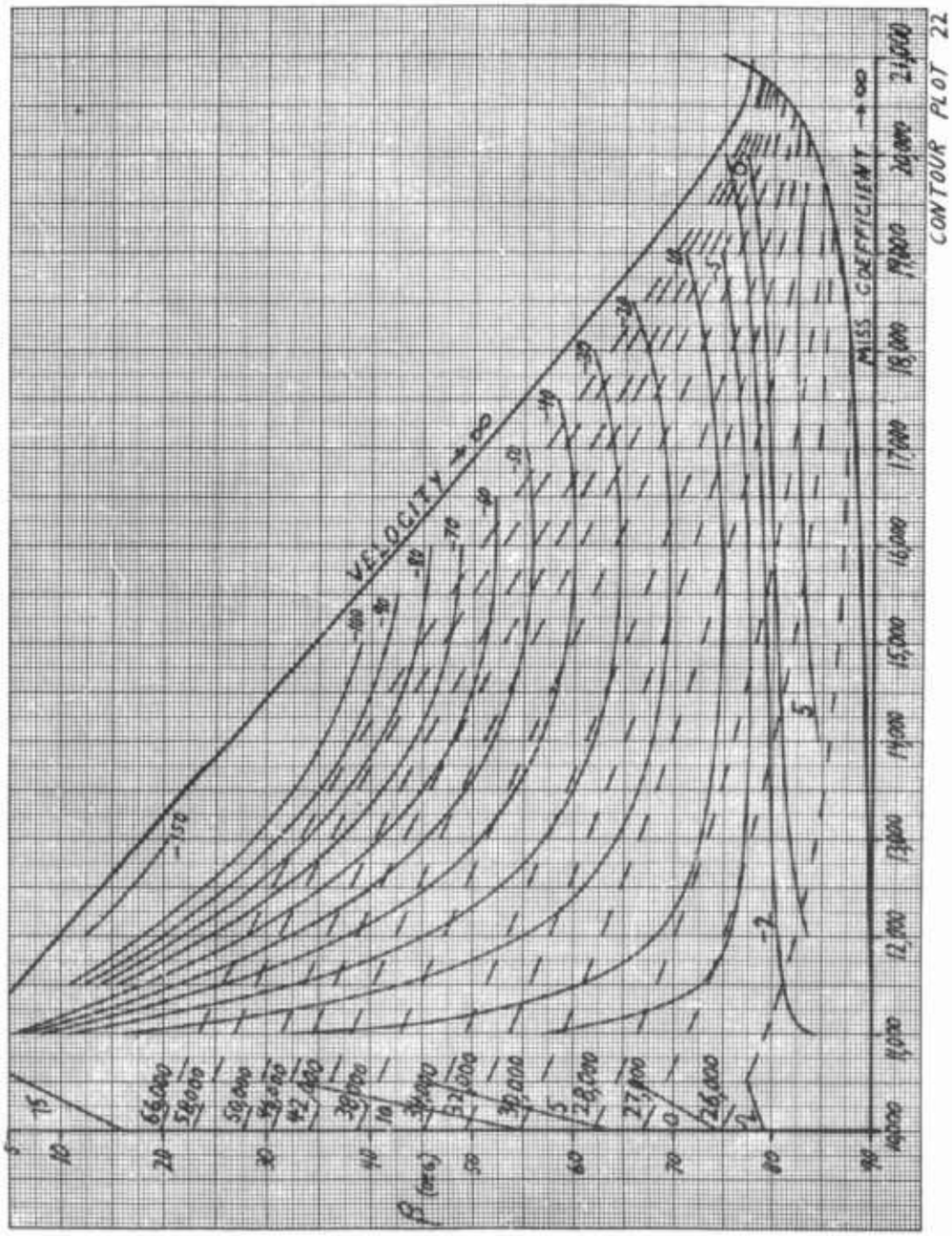
CONTOUR PLOT 22
VELOCITY → ∞
MASS COEFFICIENT → ∞
β (DEG.)

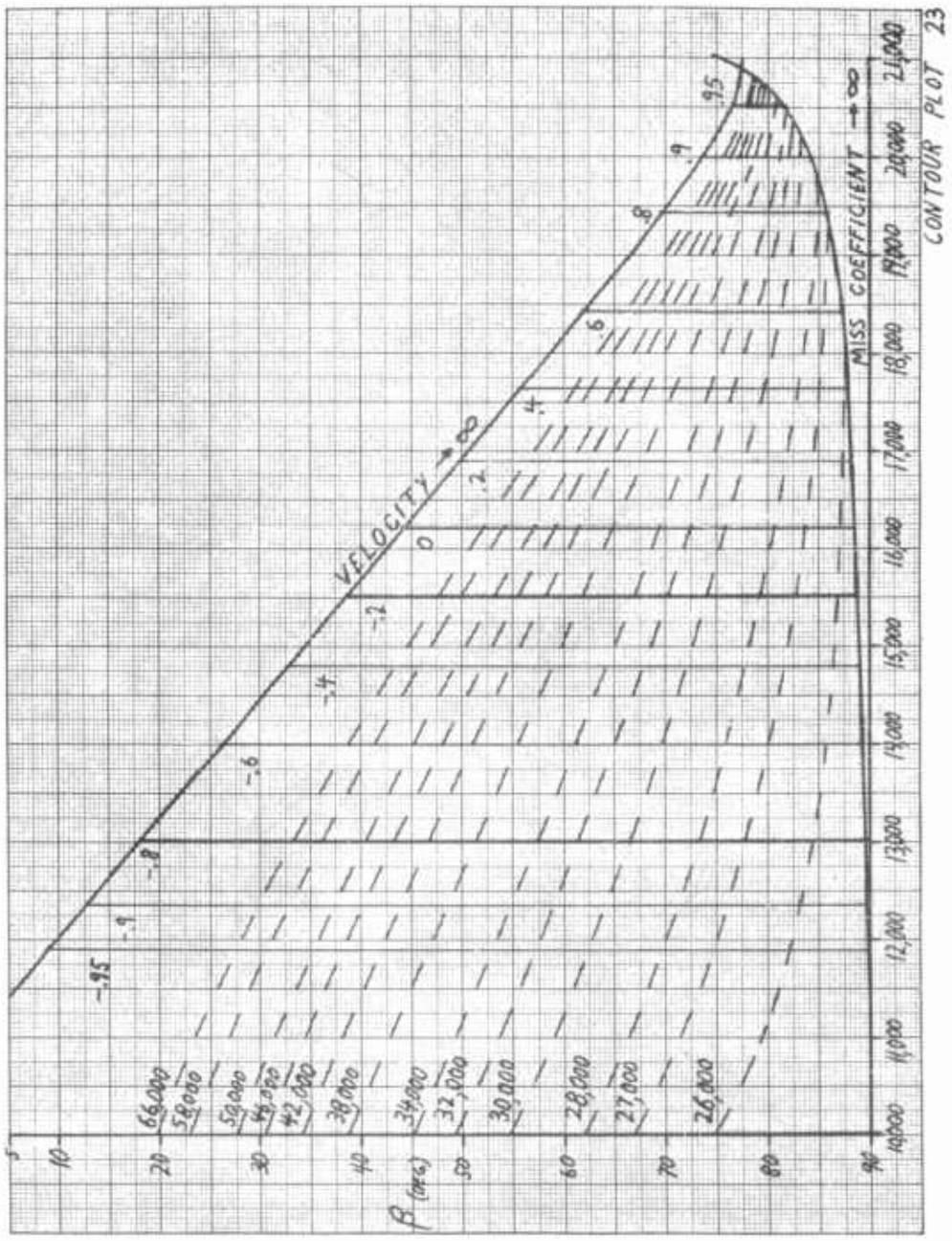
CONTOUR PLOT 23
MISS COEFFICIENT → ∞
VELOCITY → ∞
.95
.9
.8
.6
.4
.2
0
-.2
-.4
-.6
-.8
-.9
-.95
66,000
58,000
50,000
46,000
42,000
38,000
34,000
32,000
30,000
28,000
27,000
26,000
β (DEG.)
5
10
20
30
40
50
60
70
80
90
21,000
20,000
19,000
18,000
17,000
16,000
15,000
14,000
13,000
12,000
11,000
10,000

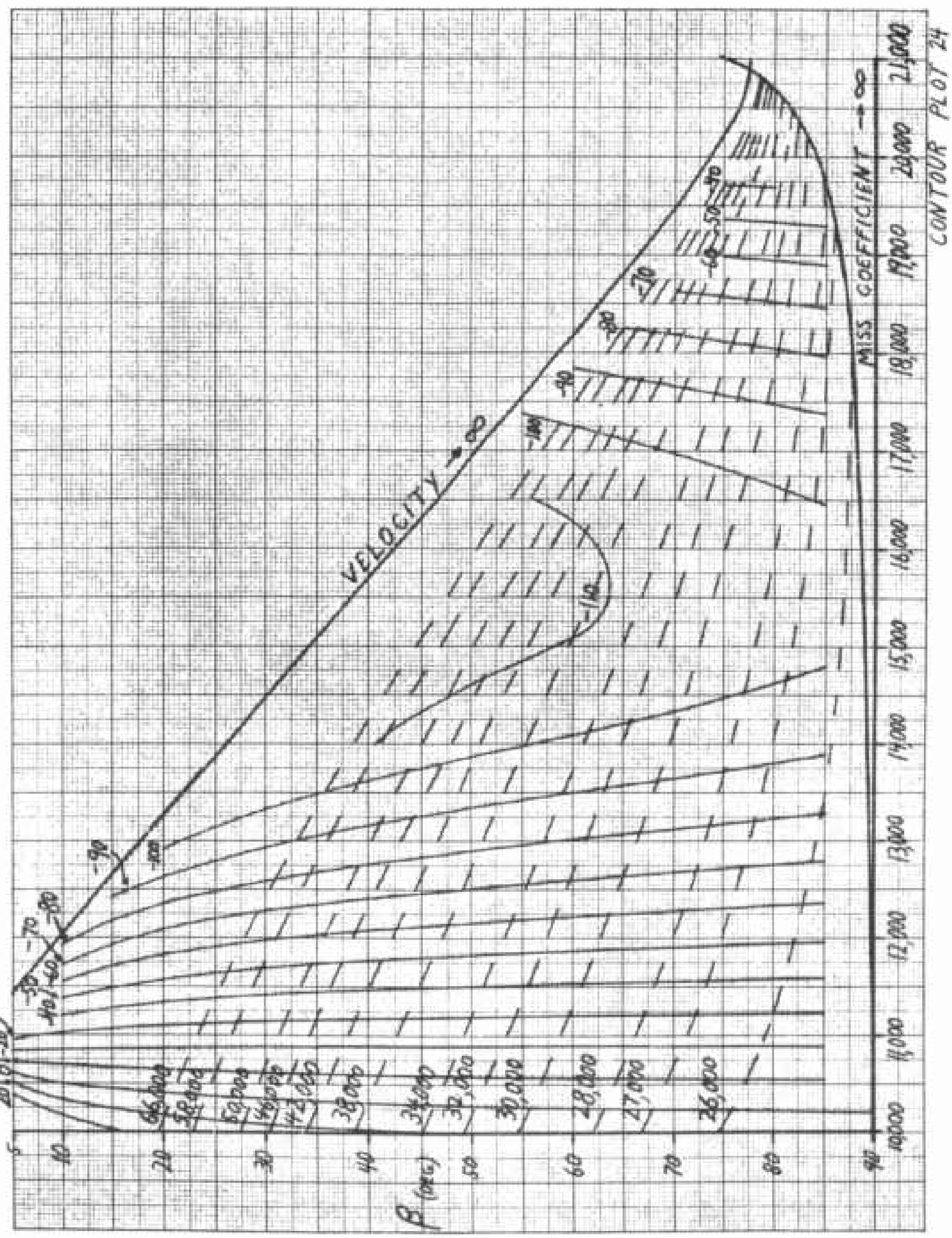
VELOCITY → ∞
MISS COEFFICIENT → ∞
CONTOUR PLOT 24
β (DEG)

INTERNAL DISTRIBUTION

J. A. Aseltine
J. M. Baker
G. Bartos
P. O. Bell
B. H. Billik
B. H. Billings
P. Bos
H. S. Braham
R. R. Brown
R. J. Farrar
T. P. Gabbard
E. U. Gambaro
E. A. Goldberg
R. C. Gore
A. B. Greenberg
P. T. Guttman
N. S. Hall
A. R. Jacobsen
J. P. Jones
H. K. Karrenberg
L. Kulakowski
E. Levin
W. W. Loft
R. D. Luders
M. L. Luther
R. J. Mercer
J. E. Michaels
A. H. Milstead
H. Nakamura
J. M. Nilles
F. M. Perkins
J. E. Pierson
C. M. Price
W. F. Reichert
J. R. Rogers
H. L. Roth
L. B. Russak
K. Walker, Jr.
E. T. Welmers

Central Files
ASRDG

San Bernardino Operations

G. W. Anderson
F. Augustine
D. Y. Barrer
J. W. Capps
A. B. Chatfield
W. Dorrance
E. Durand
J. J. Jerger
R. W. Kafka
S. A. Levine
M. Masaki
R. J. McGrath
G. P. Millburn
R. F. Newbold
N. B. Nichols
A. K. Ohashi
W. Portenier
S. Rosenzweig
M. Ruttmann
P. W. Snyders
R. E. Trudel
W. C. Yengst
K. Young

EXTERNAL DISTRIBUTION

J. E. Bekius, Maj (SSOW)

H. A. Courtney, Maj (SP-11)

BSD - Norton AFB

LtCol W. R. Manlove, BSRGA

Capt G. E. Danforth, BSRGA-1

Capt R. A. Dodson, GSPN

Lt Sill, BSFP

Capt J. E. Dalton, BSRGA-1 (LA)
Research and Development Center

Defense Documentation Center
Cameron Station
Alexandria, Virginia

UNCLASSIFIED